

Electronic Supplementary Information (ESI) for Chemical Science

Supporting Information

Efficient circularly polarized multiple resonance thermally activated delayed fluorescence from B,N-embedded hetero[8]helicene enantiomers

Tingting Huang,^{#,a} Li Yuan,^{#,c} Xueying Lu,^a Yupei Qu,^a Cheng Qu,^a Yincai Xu,^{*,a} You-Xuan Zheng^{*,c} and Yue Wang^{*,a,b}

^a T. Huang, X. Lu, Y. Qu, Dr. C. Qu, Dr. Y. Xu and Prof. Y. Wang

State Key Laboratory of Supramolecular Structure and Materials, College of Chemistry
Jilin University, Changchun 130012, P. R. China

E-mails: yc xu17@mails.jlu.edu.cn; yuewang@jlu.edu.cn

^b Prof. Y. Wang

Jihua Laboratory, 28 Huandao Nan Road, Foshan, 528200, Guangdong Province, P. R. China.

^c L. Yuan and Prof. Y.-X. Zheng

State Key Laboratory of Coordination Chemistry, Jiangsu Key Laboratory of Advanced Organic
Materials, School of Chemistry and Chemical Engineering

Nanjing University, Nanjing 210023, P. R. China

E-mail: yxzheng@nju.edu.cn

General Information: Thermo Fisher ITQ1100 GC/MS mass spectrometer was employed to measure the mass spectra. And Matrix-assisted laser desorption time-of-flight mass spectrometry (MALDI-TOF-MS) based on Bruker Autoflex Speed was also employed to measure the mass spectra, and trans-2-[3-(4-*tert*-butylphenyl)-2-methyl-2-propenylidene]malononitrile (DCTB) was used as the matrix. Bruker AVANCE III 500 and 600 MHz spectrometers were selected to measure the ^1H and $^{13}\text{C}\{^1\text{H}\}$ NMR spectra, with tetramethylsilane (TMS) as the internal standard. Shimadzu RF-5301 PC spectrometer and Shimadzu UV-2550 spectrophotometer were adopted to record the PL emission spectra and UV-Vis absorption, respectively. The fluorescence and phosphorescence spectra taken at liquid nitrogen temperature (77 K) were recorded by Ocean Optics QE Pro with a 365 nm Ocean Optics LLS excitation source. Edinburgh FLS920 steady state fluorimeter equipping with an integrating sphere was employed to measure the absolute photoluminescence quantum yields of both solution and films. BOF-5-50 vacuum sublimation instrument (AnHui BEQ Equipment Technology CO., Ltd) was used to sublime the target compound. In the range of 25 to 800 °C, TA Q500 thermogravimeter was selected to perform the thermogravimetric analysis (TGA) under nitrogen atmosphere at a heating rate of 10 K min $^{-1}$. BAS 100W Bioanalytical electrochemical work station was used to measure the electrochemical property with platinum disk as working electrode, platinum wire as auxiliary electrode, a porous glass wick Ag/Ag $^+$ as pseudo reference electrode and ferrocene/ferrocenium as the internal standard. And 0.1 M solution of *n*-Bu₄NPF₆ was utilized as the supporting electrolyte to measure the oxidation (in anhydrous dichloromethane) or reduction (in anhydrous tetrahydrofuran) potentials at a scan rate of 100 mV s $^{-1}$ with a sample solution concentration of 2×10^{-3} M. FLS980 fluorescence lifetime measurement system with 365 nm LED excitation source was selected to investigate the transient PL decay. DAICEL CHIRAL TECHNOLOGIES (CHINA) CO., LTD. was commissioned to accomplish the chiral resolution of racemic BN-TP-ICz using a CHIRALPAK IE-3 (IE30CE-XB011) high performance liquid chromatography (HPLC) column and the chiral test of the residue samples (after thermal evaporation of the enantiomer under vacuum) using a CHIRALPAK IE (IE00CE-BS027) HPLC column. Circular dichroism (CD) spectra were measured by a Jasco J-810 circular dichroism spectrometer with “Standard” sensitivity. Circularly polarized photoluminescence (CPPL) and circularly polarized electroluminescence (CPEL) spectra were

measured on a Jasco CPL-300 spectrophotometer with “Standard” sensitivity at scan speed of 100 nm min⁻¹ and respond time of 4.0 s employing “slit” mode. Experimental characteristic of the emitting dipole orientation was performed by R1-OLED system (ideaoptics CO., Ltd). The emitting dipole orientation was then determined by least-square fitting of the measured angle-dependent *p*-polarized emission intensity with calculated results.

Single Crystal Structure: Single crystal was collected on Rigaku RAXIS-PRID diffractometer using the ω -scan mode with graphite monochromator Mo•K α radiation. The crystal was kept at 295.0 K during data collection. Using Olex2¹, the structure was solved with the XT² structure solution program using Intrinsic Phasing and refined with the XL³ refinement package using Least Squares minimisation.

Theoretical Calculations Method: The ground state geometries and the lowest triplet (T_1) state geometries of gas state were fully optimized by B3LYP method including Grimme’s dispersion correction with 6-31G(d,p) basis set using Gaussian 16 software package.⁴⁻⁹ HOMO and LUMO were visualized with Gaussview 6.0. The excited state properties were calculated by TDDFT with the same theory level as DFT. The transition state was calculated at the B3LYP-D3(BJ)/6-31G(d,p) level, and frequency calculations at the same level were performed to verify stationary as transition state (with only one imaginary frequency). The triplet spin density distribution (TSDD) analysis, LOL- π analysis, hole–electron analysis and noncovalent interactions analysis (RDG) and TDM analysis were completed with Multiwfn program.¹⁰ The drawing of LOL- π isosurface, hole and electron distribution plot, RDG isosurface, the calculation of RMSD and the plot of TDM vector were completed with VMD 1.9.4.¹¹

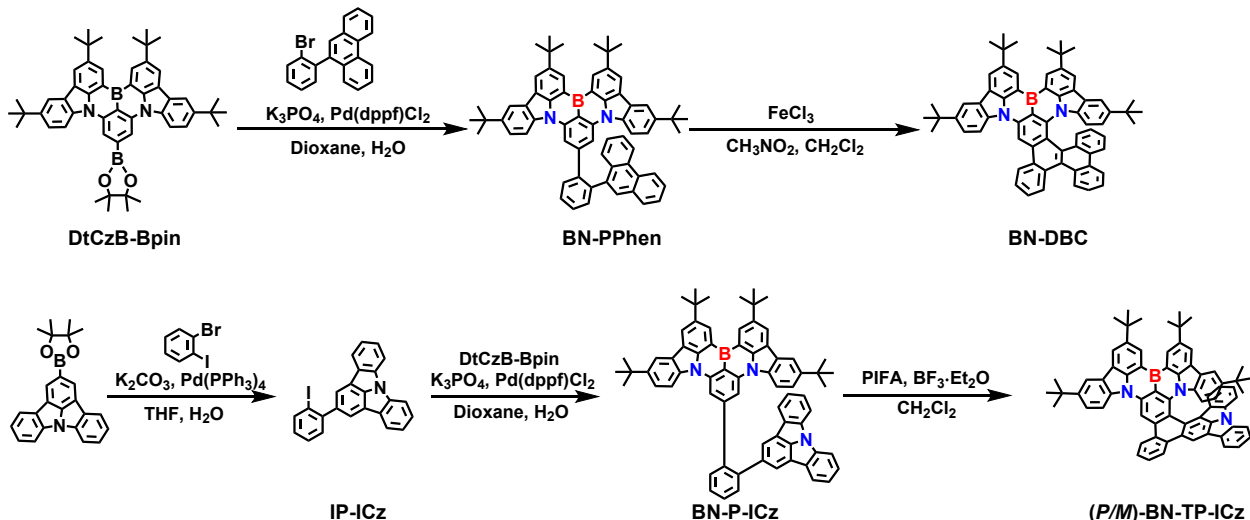
Calculation of Reorganization Energies: The reorganization energies consist of the external and internal reorganization energy.¹²⁻¹³ The external reorganization energy caused by the polarization of the medium can be negligible.¹⁴⁻¹⁵ The internal reorganization energy is caused by the geometrical deformation in the Franck–Condon vertical absorption transition and radiative process, and the value can be estimated as the following:¹⁶

$$\lambda = \lambda_{S0} + \lambda_{S1} = [E^{S0}(S_1) - E^{S0}(S_0)] + [E^{S1}(S0) - E^{S1}(S1)] \quad (S1)$$

Here, $E^{S0}(S_1)$ is the energy of the S_0 state with the optimized S_1 geometry, $E^{S0}(S_0)$ is the energy of the S_0 state with the optimized S_0 geometry, $E^{S1}(S_0)$ is the energy of S_1 state with the optimized

S_0 geometry, and $E^{S^1}(S_1)$ is the energy of S_1 state with the optimized S_1 geometry. The single point energy was calculated at B3LYP level with 6-31G(d,p) basis set.

Synthesis of Materials: All reagents were purchased from *Energy Chemical Co.* and *Nanjing Kaimuco Technology Co., Ltd* and immediately used without further purification. The Schlenk technology was strictly performed under nitrogen condition in all reactions and the concrete synthetic procedures were showed below in detail. The final products were first purified by column chromatography, then temperature-gradient sublimation was utilized to further purify the target compounds under high vacuum to obtain highly pure samples.



Scheme S1. Synthetic procedures of BN-DBC and (P/M)-BN-TP-ICz.

Synthesis of DtCzB-Bpin: The synthetic process was referred to the reported literature.¹⁷

Synthesis of BN-PPhen: 9-(2-Bromophenyl)phenanthrene (0.87 g, 2.62 mmol), DtCzB-Bpin (1.00 g, 1.31 mmol) and potassium phosphate (K_3PO_4) (0.83 g, 3.93 mmol) were added with water (94.0 μ L, 5.22 mmol) and dioxane (30 mL). The mixture was bubbled with nitrogen for 5 minutes, and dichloro[1,1'-bis(diphenylphosphino)ferrocene]palladium(II) ($Pd(dppf)Cl_2$) (0.30 g, 0.04 mmol) was added under high nitrogen flow. Then the mixture was heated to 90 °C and stirred for 16 hours. After cooling to room temperature, the reaction mixture was extracted with dichloromethane and water, and the combined organic layer was condensed in vacuum, and then the crude product was further purified by column chromatography with a mixture eluent of petroleum ether/dichloromethane (2:1) to afford a yellow solid (0.76 g). Yield: 65%. 1H NMR (500

MHz, Chloroform-*d*) δ 9.00 (d, *J* = 1.9 Hz, 2H), 8.59 – 8.53 (m, 2H), 8.36 (d, *J* = 1.8 Hz, 2H), 8.16 (s, 2H), 8.12 (d, *J* = 2.0 Hz, 2H), 8.05 (dd, *J* = 8.2, 1.5 Hz, 1H), 7.97 – 7.92 (m, 2H), 7.87 (dd, *J* = 7.7, 1.5 Hz, 1H), 7.74 – 7.71 (m, 1H), 7.71 – 7.67 (m, 1H), 7.65 (td, *J* = 7.4, 1.5 Hz, 1H), 7.60 – 7.53 (m, 2H), 7.52 – 7.43 (m, 4H), 7.10 (dd, *J* = 8.7, 2.1 Hz, 2H), 1.61 (s, 18H), 1.47 (s, 18H). ESI-MS (M): m/z: 892.43 [M]⁺ (calcd: 892.49).

Synthesis of BN-DBC: BN-PPhen (0.50 g, 0.56 mmol) was dissolved in 30 mL extra dry dichloromethane, and iron(III) chloride (0.91 g, 5.6 mmol) was dissolved in 13 mL nitromethane and placed in separating funnel. The mixture was bubbled with nitrogen for 5 minutes. Then iron trichloride suspension was added slowly in ice water bath, after dropping, the ice water bath was removed, and the reaction system was kept at room temperature for 2 hours. 8 mL methanol and 8 mL water were added to quench the reaction, the mixture was extracted with dichloromethane and water, and the combined organic layer was condensed in vacuum, and then the crude product was further purified by column chromatography with a mixture eluent of petroleum ether/dichloromethane (2:1) to afford an orange solid (0.41 g). Yield: 82%. ¹H NMR (500 MHz, Chloroform-*d*) δ 9.65 (d, *J* = 6.8 Hz, 1H), 9.17 (dd, *J* = 5.7, 1.8 Hz, 2H), 9.13 (d, *J* = 7.7 Hz, 1H), 9.02 (td, *J* = 8.1, 3.2 Hz, 2H), 8.80 (dd, *J* = 8.8, 4.2 Hz, 1H), 8.54 (d, *J* = 1.8 Hz, 1H), 8.44 (d, *J* = 8.1 Hz, 1H), 8.37 (d, *J* = 2.0 Hz, 1H), 8.27 (d, *J* = 1.7 Hz, 1H), 8.11 (d, *J* = 8.1 Hz, 1H), 7.90 – 7.85 (m, 2H), 7.82 – 7.76 (m, 2H), 7.70 (dd, *J* = 8.4, 6.9 Hz, 1H), 7.57 (d, *J* = 2.0 Hz, 1H), 7.07 (ddt, *J* = 8.1, 6.8, 1.1 Hz, 1H), 7.04 – 7.00 (m, 1H), 6.57 (ddt, *J* = 8.2, 6.9, 1.2 Hz, 1H), 6.18 (dd, *J* = 8.7, 4.0 Hz, 1H), 5.82 (dt, *J* = 8.7, 2.2 Hz, 1H), 1.76 – 1.66 (m, 18H), 1.60 (s, 9H), 1.16 (s, 9H). ¹³C{¹H} NMR (151 MHz, Chloroform-*d*) δ 145.4, 145.2, 144.7, 144.3, 141.9, 141.8, 141.5, 140.8, 138.5, 138.4, 135.5, 131.3, 131.0, 130.4, 130.2, 129.6(8), 129.6(6), 129.0, 128.8, 128.6, 128.3(0), 128.2(6), 127.8, 127.3, 126.7(4), 126.6(5), 126.3, 125.9, 125.8, 125.7, 125.3, 125.1, 124.9, 124.7, 124.5, 124.1, 123.6, 122.0, 121.8, 121.7, 121.0, 120.7, 117.5, 115.2, 113.9, 112.2, 109.9, 101.3, 35.3, 35.2, 34.9, 34.4, 32.3, 32.2, 31.9, 31.5. MALDI-TOF-MS (M): 890.515 [M]⁺ (calcd: 890.477). Anal. Calcd for C₆₆H₅₉BN₂: C, 88.97; H, 6.67; N, 3.14. Found: C, 89.20; H, 6.73; N, 3.14.

Synthesis of IP-ICz: 2-(4,4,5,5-Tetramethyl-1,3,2-dioxaborolan-2-yl)indolo[3,2,1-*jk*]carbazole (1.42 g, 3.90 mmol), 1-bromo-2-iodobenzene (3.30 g, 11.70 mmol) and K₂CO₃ (1.62 g, 11.70

mmol) were added with water (3 mL) and tetrahydrofuran (THF) (30 mL). The mixture was bubbled with nitrogen for 5 minutes, and tetrakis(triphenylphosphine)palladium(0) ($\text{Pd}(\text{PPh}_3)_4$) (0.08 g, 0.07 mmol) was added under high nitrogen flow. Then the mixture was heated to 80 °C and stirred for 14 hours. After cooling to room temperature, the reaction mixture was extracted with dichloromethane and water, and the combined organic layer was condensed in vacuum, and then the crude product was further purified by column chromatography with a mixture eluent of petroleum ether/dichloromethane (20:1) to afford a white solid (1.27 g). Yield: 73%. ^1H NMR (500 MHz, $\text{DMSO}-d_6$) δ 8.35 – 8.31 (m, 4H), 8.19 (s, 2H), 7.83 (dd, J = 8.0, 1.3 Hz, 1H), 7.66 (ddd, J = 8.4, 7.4, 1.2 Hz, 2H), 7.61 (dd, J = 7.6, 1.8 Hz, 1H), 7.54 (td, J = 7.4, 1.3 Hz, 1H), 7.44 (td, J = 7.6, 1.0 Hz, 2H), 7.40 (td, J = 7.7, 1.8 Hz, 1H). ESI-MS (M): m/z: 444.48 [M] $^+$ (calcd: 443.02).

Synthesis of BN-P-ICz: BN-P-ICz was synthesized in the same way of preparing BN-PPhen, just replaced 9-(2-bromophenyl)phenanthrene with equivalent stoichiometric IP-ICz.

BN-P-ICz: Yellow solid (0.93 g). Yield: 74%. ^1H NMR (500 MHz, $\text{DMSO}-d_6$) δ 8.94 (s, 2H), 8.74 (d, J = 2.1 Hz, 2H), 8.47 (s, 2H), 8.40 (d, J = 2.3 Hz, 2H), 8.29 (d, J = 7.9 Hz, 2H), 8.25 – 8.19 (m, 4H), 7.98 (s, 1H), 7.85 (d, J = 7.0 Hz, 1H), 7.73 (d, J = 6.7 Hz, 2H), 7.56 (t, J = 7.8 Hz, 2H), 7.47 (d, J = 9.1 Hz, 2H), 7.33 (t, J = 7.6 Hz, 2H), 7.14 (d, J = 8.6 Hz, 2H), 1.58 (s, 18H), 1.30 (s, 18H). MALDI-TOF-MS (M): m/z: 955.367 [M] $^+$ (calcd: 955.50).

Synthesis of (P/M)-BN-TP-ICz: BN-P-ICz (0.90 g, 0.94 mmol) was dissolved in 20 mL extra dry dichloromethane, followed by bubbling the mixture with nitrogen for 5 minutes. Then [bis(trifluoroacetoxy)iodo]benzene (PIFA) (0.45 g, 1.04 mmol) was added under a high flow of nitrogen. Next, boron trifluoride etherate ($\text{BF}_3 \cdot \text{Et}_2\text{O}$) (0.30 g, 2.08 mmol, 46.5 wt%) was slowly added to the mixture solution at –40 °C under nitrogen atmosphere. The resulting mixture was kept stirred at –40 °C for 1.5 hours and monitored by thin layer chromatography until the reaction was complete. The system was returned to room temperature, 2 mL of methanol was added to quench the reaction, and then the solvent was removed by rotary evaporation. The mixture was extracted with dichloromethane and water, and the combined organic layers were condensed in vacuum, and then further purified by column chromatography with a mixture eluent of petroleum ether/dichloromethane (6:1) to afford a yellow powder (0.56 g). Yield: 62%. ^1H NMR

(500 MHz, Chloroform-*d*) δ 9.50 (s, 1H), 9.37 (s, 1H), 9.22 (dd, J = 5.8, 1.8 Hz, 2H), 9.07 (d, J = 8.0 Hz, 1H), 8.95 (d, J = 8.0 Hz, 1H), 8.76 (d, J = 8.7 Hz, 1H), 8.59 (d, J = 1.8 Hz, 1H), 8.39 (d, J = 2.0 Hz, 1H), 8.28 (d, J = 7.5 Hz, 1H), 8.13 (d, J = 1.7 Hz, 1H), 7.91 (t, J = 7.2 Hz, 1H), 7.86 (dd, J = 8.7, 2.0 Hz, 2H), 7.68 (d, J = 7.9 Hz, 1H), 7.55 (d, J = 2.0 Hz, 1H), 7.52 – 7.49 (m, 1H), 7.43 (d, J = 7.9 Hz, 1H), 7.38 (td, J = 7.5, 1.0 Hz, 1H), 7.02 – 6.98 (m, 1H), 6.86 (d, J = 7.8 Hz, 1H), 6.35 (dd, J = 8.8, 2.0 Hz, 1H), 6.14 (d, J = 8.8 Hz, 1H), 6.10 – 6.07 (m, 1H), 1.77 (s, 9H), 1.72 (s, 9H), 1.64 (s, 9H), 0.98 (s, 9H). ^{13}C NMR (151 MHz, Chloroform-*d*) δ 145.6, 145.3, 145.0, 144.7, 144.0, 142.4, 142.2, 141.7, 140.9, 139.8, 138.5, 137.6, 137.1, 136.3, 134.1, 130.1, 129.9, 129.37, 129.3, 128.9, 128.6, 127.3, 126.8, 126.6, 126.2, 125.9, 125.5, 125.3, 124.7, 124.5, 124.2, 123.8, 123.5, 123.1, 122.9, 121.9, 121.7, 121.5, 120.8, 120.7, 119.9, 117.7, 117.5, 115.1, 115.0, 113.8, 113.1, 111.9, 111.2, 110.4, 101.2, 35.3, 34.9, 34.2, 32.3, 32.2, 31.9, 31.2. MALDI-TOF-MS (M): m/z: 953.497 [M]⁺ (calcd: 953.49). Anal. Calcd for $\text{C}_{70}\text{H}_{60}\text{BN}_3$: C, 88.12; H, 6.34; N, 4.40. Found: C, 88.74; H, 6.36; N, 4.39. Anal. Calcd for $\text{C}_{66}\text{H}_{70}\text{BN}_3$: C, 86.53; H, 7.70; N, 4.59. Found: C, 87.03; H, 7.63; N, 4.53.

Device Fabrication and Measurements: The indium tin oxide (ITO) glass substrates with a sheet resistance of 6 Ω per square were cleaned with optical detergent, deionized water, acetone and isopropanol successively, and then treated with plasma for 5 minutes. Subsequently, they were transferred to a vacuum chamber. Under high vacuum ($< 9 \times 10^{-5}$ Pa), the organic materials were deposited onto the ITO glass substrates at a rate of 0.5 \AA s^{-1} . After finishing the deposition of organic layers, ITO glass substrates were patterned by a shadow mask with an array of 2.0 mm \times 2.5 mm openings. Then LiF and Al were successively deposited at a rate of 0.1 and 5 \AA s^{-1} , respectively. The EL spectrum, CIE coordinates and luminance intensity of OLEDs were recorded by Photo Research PR655, meanwhile, the current density (J) and driving voltage (V) were recorded by Keithley 2400. By assuming Lambertian distribution, EQE was estimated according to brightness, electroluminescence spectrum and current density. The materials of device fabrication are provided by Xi'an Polymer Light Technology Corp.

Calculation Formulas for the Photophysical Parameters: The calculation formulas for the rate constant of fluorescence (k_F), internal conversion (k_{IC}), intersystem crossing (k_{ISC}), TADF (k_{TADF}) and reverse intersystem crossing (k_{RISC}) are expressed as following list:^{18–21}

$$k_F = \Phi_F / \tau_F \quad (S2)$$

$$\Phi_{PL} = k_F / (k_F + k_{IC}) \quad (S3)$$

$$\Phi_F = k_F / (k_F + k_{IC} + k_{ISC}) \quad (S4)$$

$$\Phi_{ISC} = k_{ISC} / (k_F + k_{IC} + k_{ISC}) \quad (S5)$$

$$k_{TADF} = \Phi_{TADF} / (\Phi_{ISC} \tau_{TADF}) \quad (S6)$$

$$k_{RISC} = k_F k_{TADF} \Phi_{TADF} / (k_{ISC} \Phi_F) \quad (S7)$$

$$\Phi_{TADF}/\Phi_F = (\Phi_{ISC} \Phi_{RISC}) / (1 - \Phi_{ISC} \Phi_{RISC}) \quad (S8)$$

Where Φ_{PL} is the total fluorescence quantum yield, Φ_F is the prompt fluorescent component of Φ_{PL} , Φ_{TADF} is the delayed fluorescent component of Φ_{PL} . τ_F is the lifetime of prompt fluorescence, τ_{TADF} is the lifetime of TADF. k_F is the rate constant of fluorescence, k_{IC} is the rate constant of internal conversion; k_{TADF} , k_{ISC} , k_{RISC} are the rate constant of TADF, intersystem crossing and reverse intersystem crossing, respectively. Φ_{ISC} and Φ_{RISC} are the quantum efficiencies of ISC and RISC process, respectively.

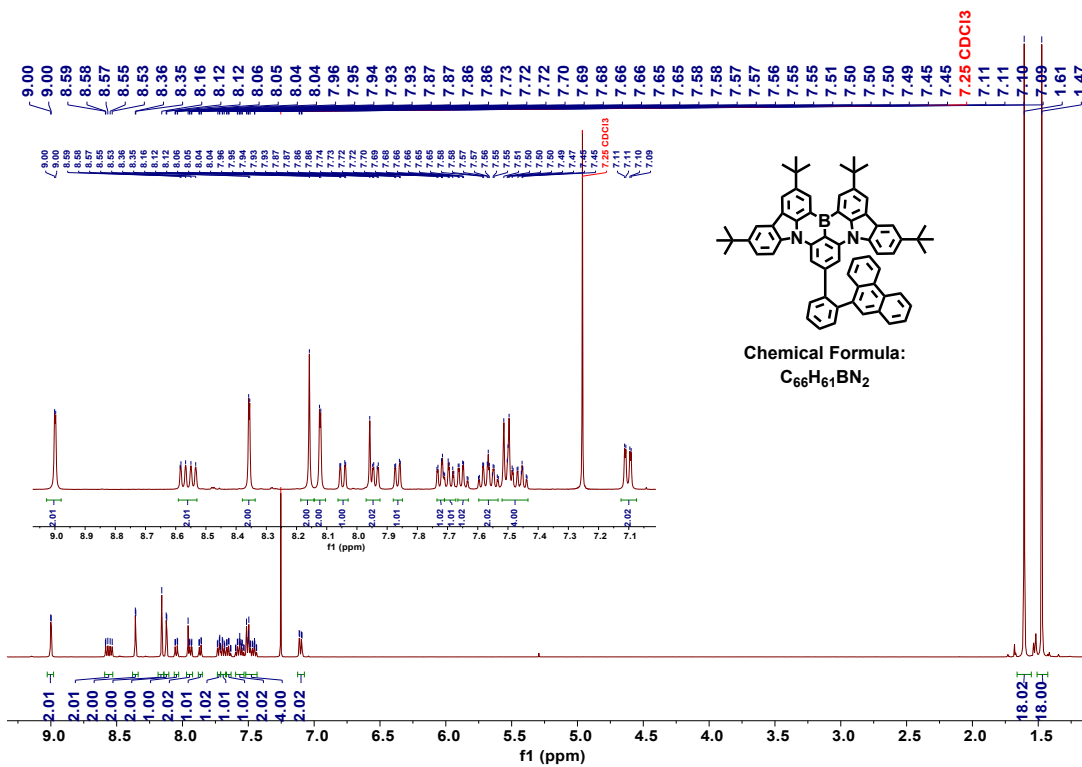


Figure S1. ^1H NMR spectrum (500 MHz, Chloroform-*d*) of BN-PPhen.

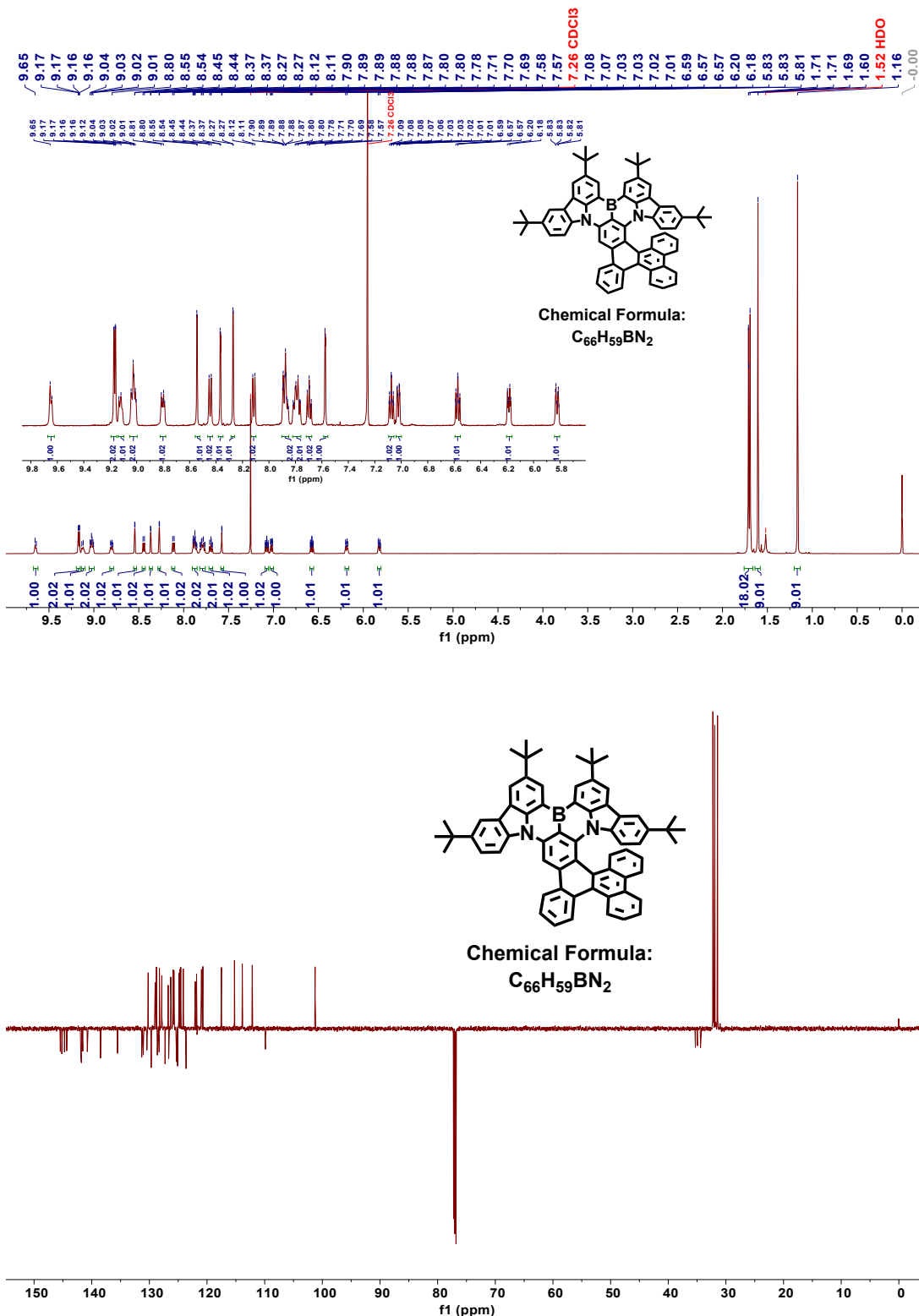


Figure S2. ^1H NMR spectrum (500 MHz, Chloroform-*d*) (top) and $^{13}\text{C}\{^1\text{H}\}$ NMR spectrum (bottom) (151 MHz, Chloroform-*d*) of BN-DBC.

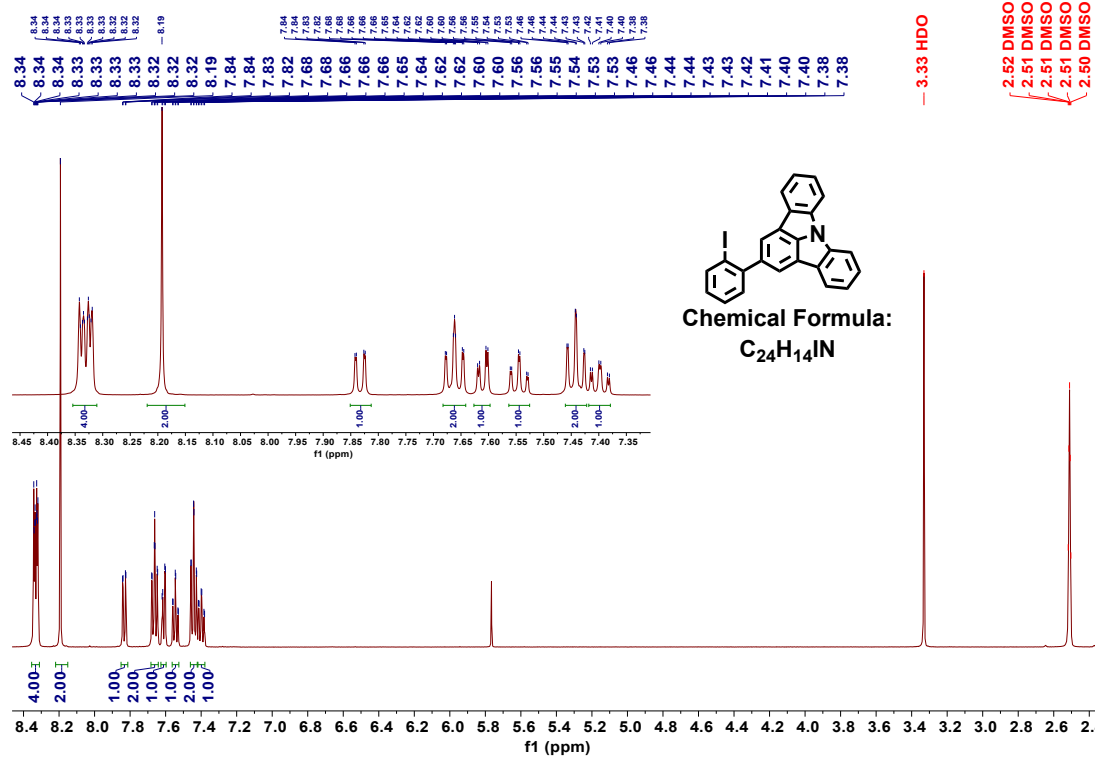


Figure S3. ^1H NMR spectrum (500 MHz, DMSO-*d*₆) of IP-ICz.

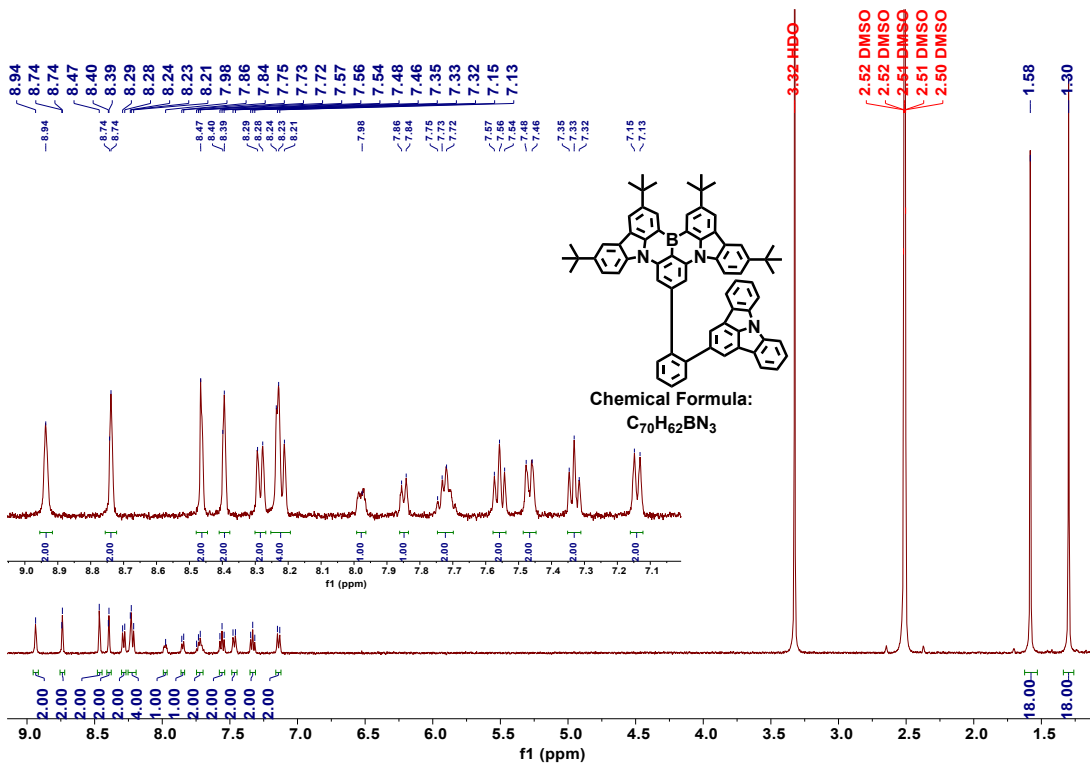
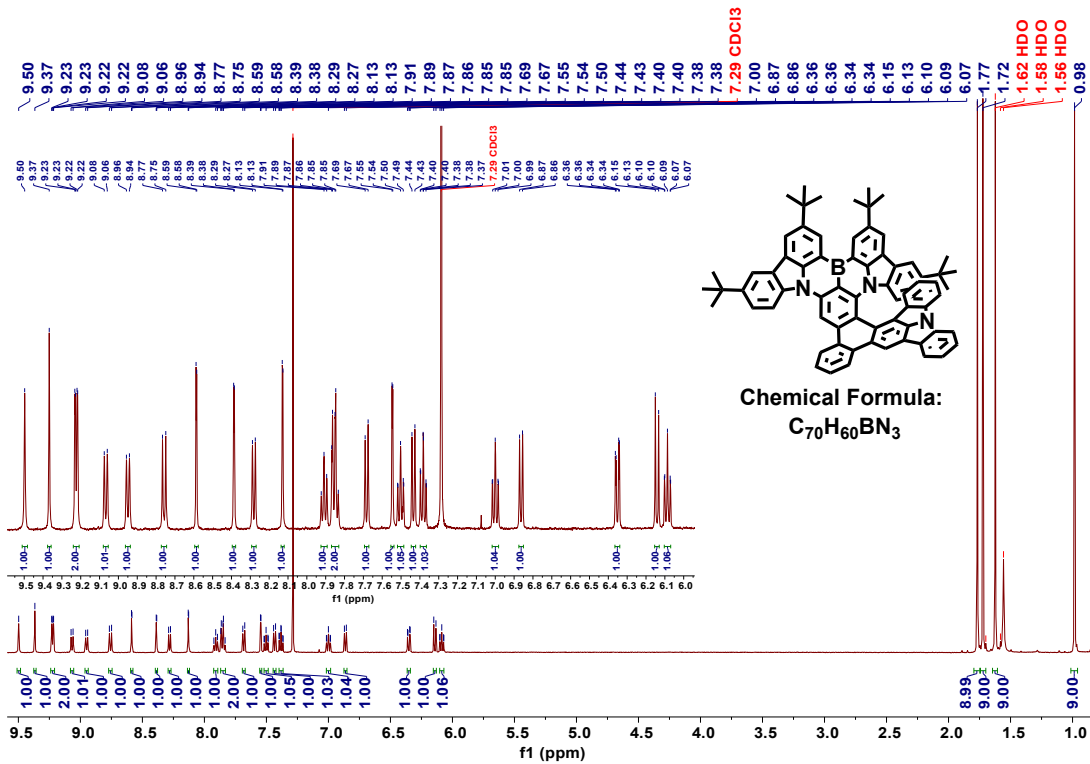


Figure S4. ¹H NMR spectrum (500 MHz, DMSO-*d*₆) of BN-P-ICz.



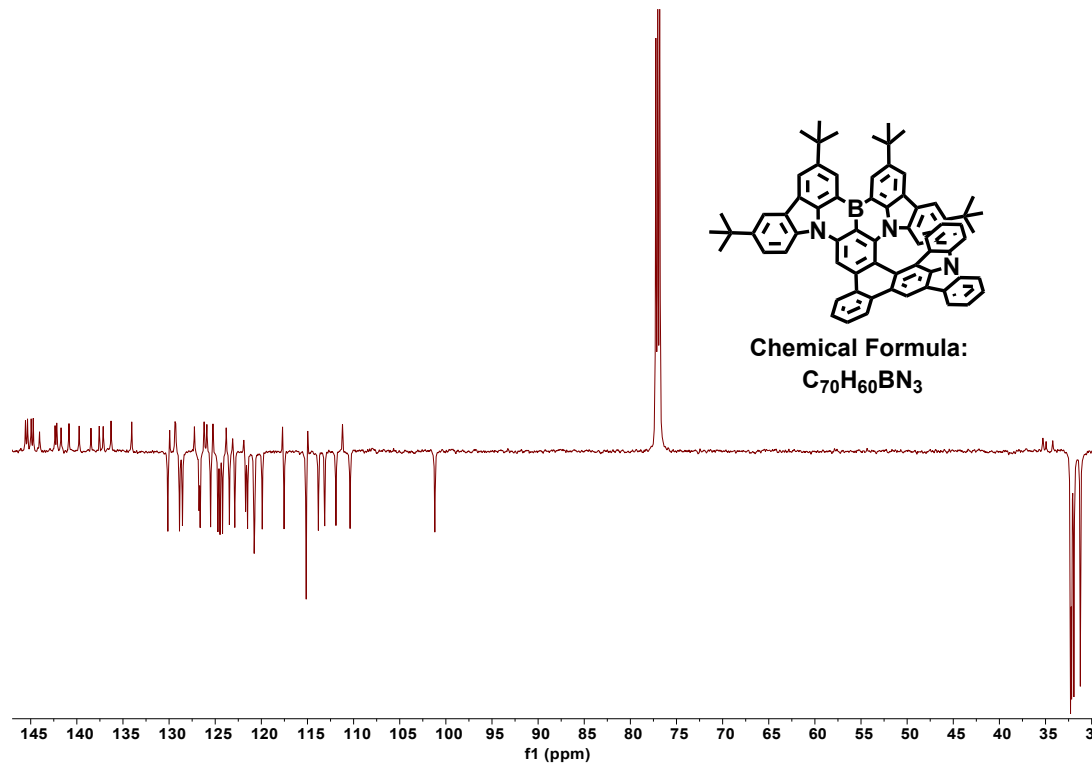


Figure S5. ^1H NMR spectrum (500 MHz, Chloroform-*d*) (top) and $^{13}\text{C}\{^1\text{H}\}$ NMR spectrum (bottom) (151 MHz, Chloroform-*d*) of BN-TP-ICz.

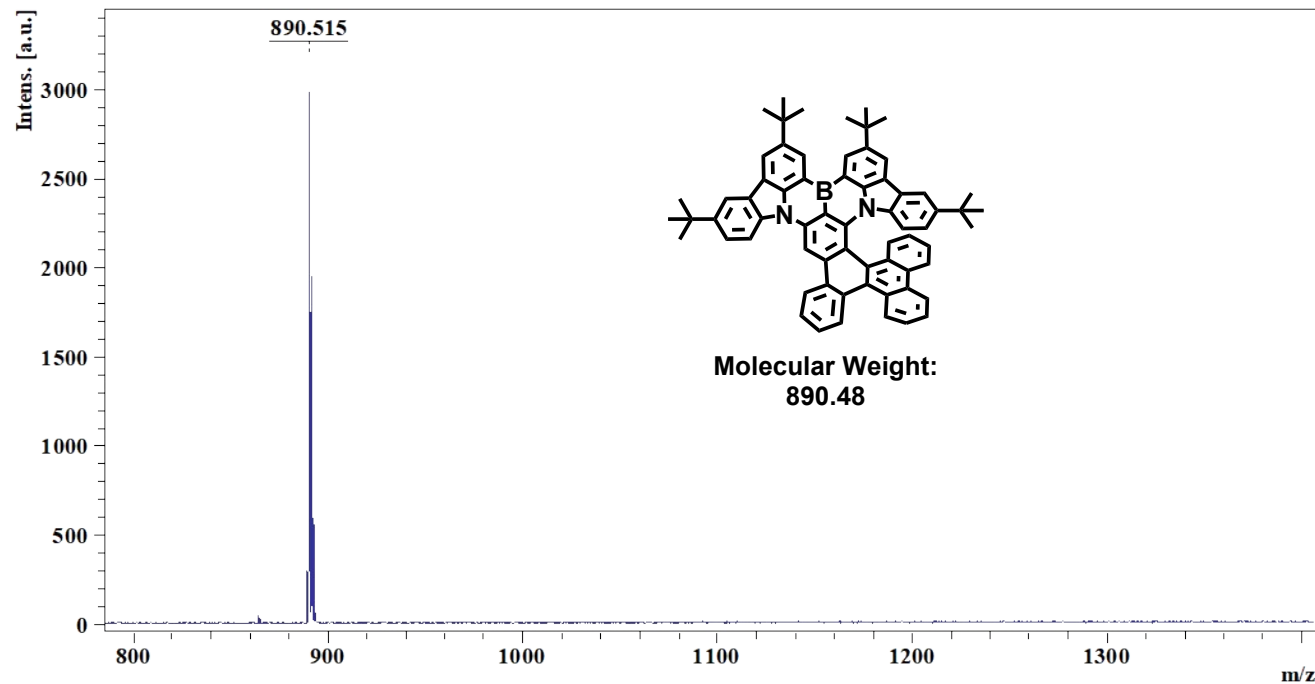


Figure S6. Mass spectrum (MALDI-TOF) of BN-DBC.

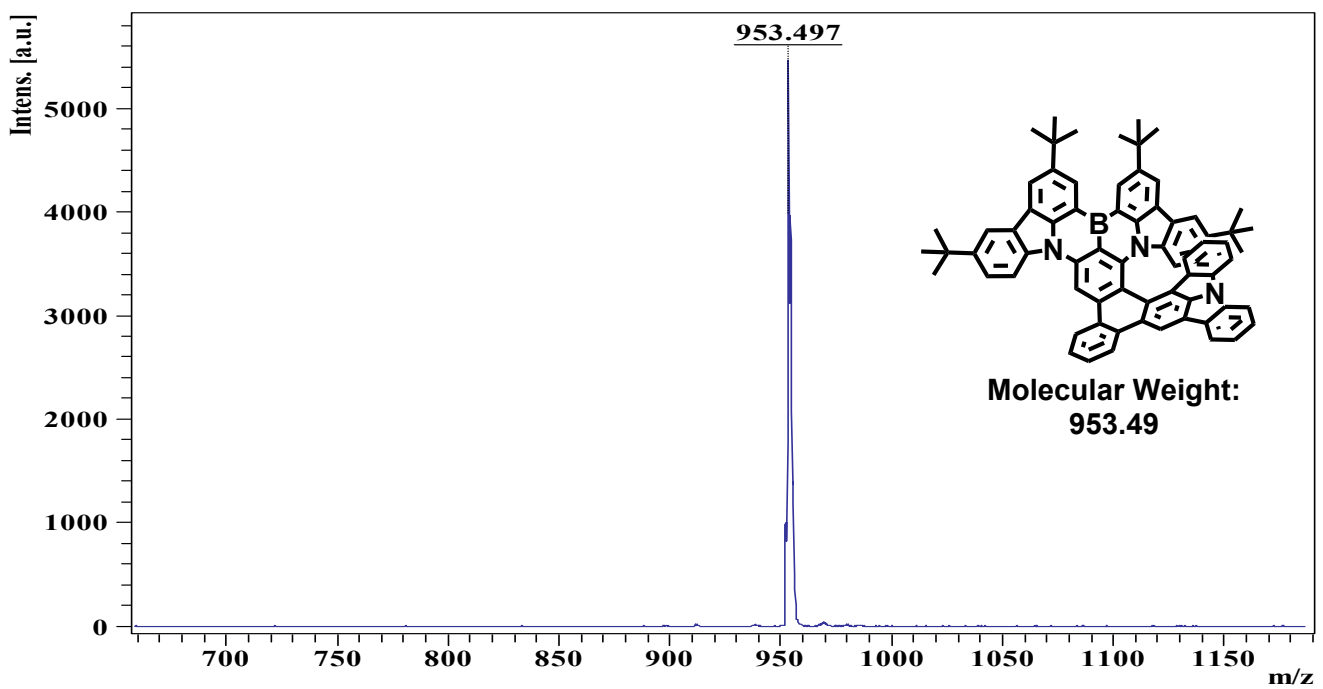


Figure S7. Mass spectrum (MALDI-TOF) of BN-TP-ICz.

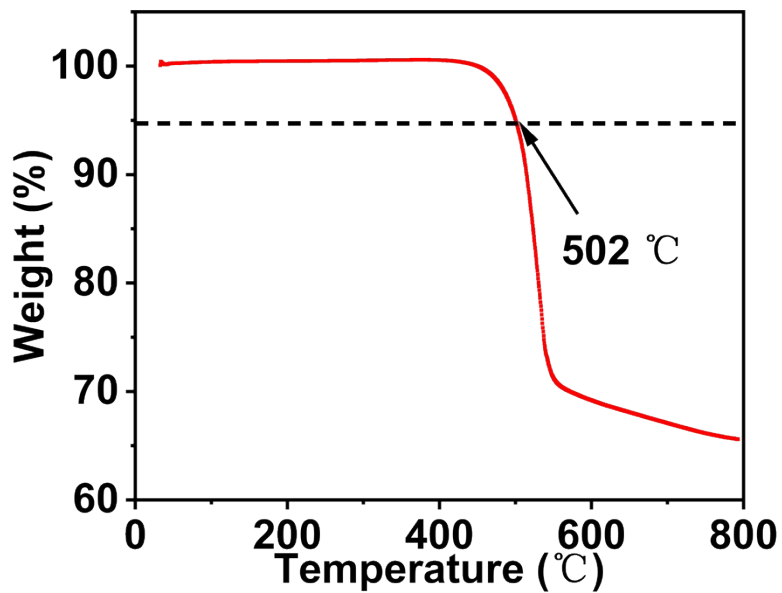


Figure S8. TGA curve of BN-TP-ICz.

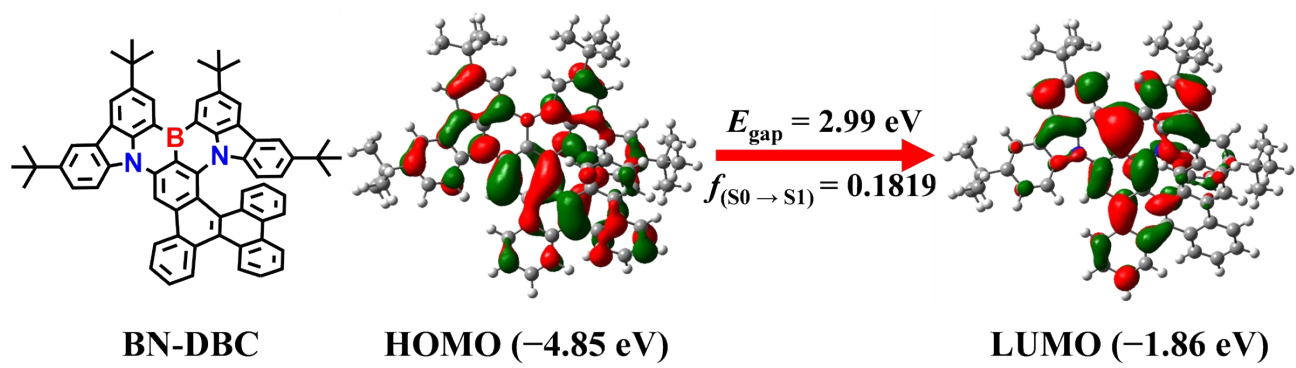


Figure S9. HOMO and LUMO distributions, HOMO–LUMO energy level gap, and oscillator strength of BN-DBC.

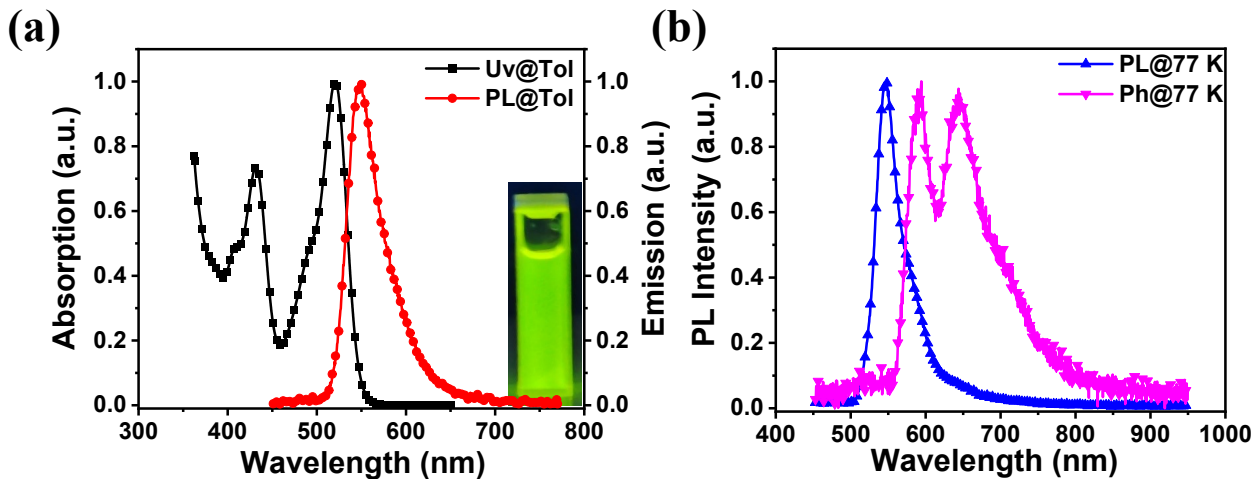


Figure S10. (a) Normalized UV–vis absorption and fluorescence spectra in toluene solution (1×10^{-5} M, 298 K) of BN-DBC. (Inset: photograph taken under 365 nm UV light). (b) Normalized fluorescence and phosphorescence spectra in toluene solution (1×10^{-5} M, 77 K) of BN-DBC.

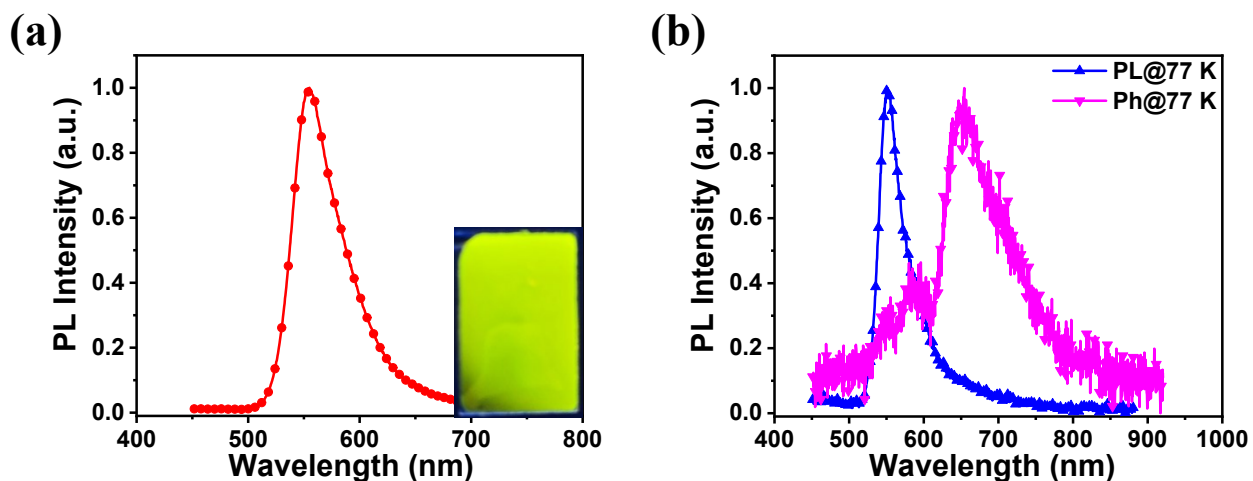


Figure S11. Normalized fluorescence spectrum (298 K, inset: photograph taken under 365 nm UV light) (a) and fluorescence and phosphorescence spectra (77 K) (b) of BN-DBC with 1 wt% doping concentration in PMMA deposited film.

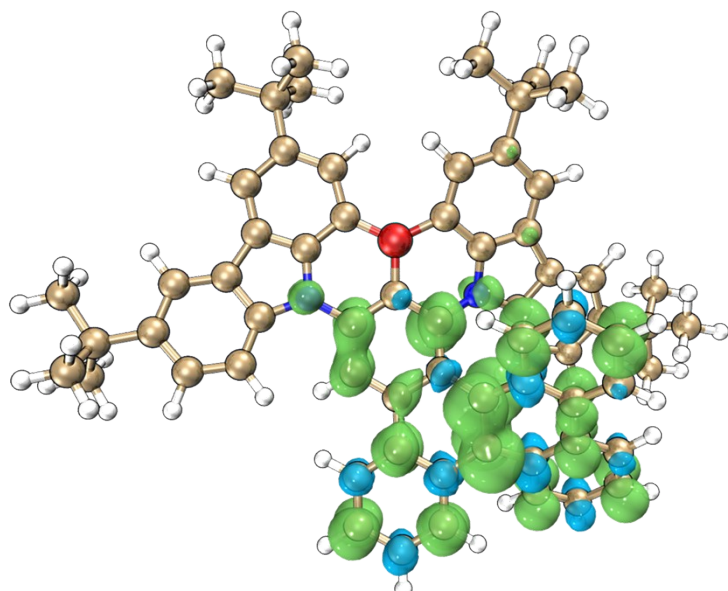


Figure S12. TSDD of BN-DBC (isovalue = 0.002).

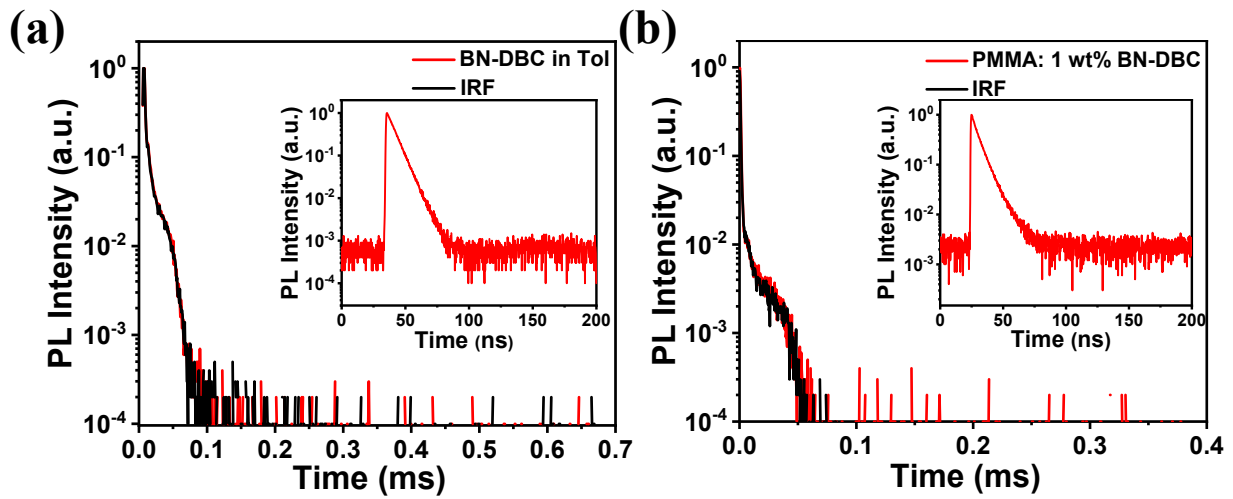


Figure S13. Transient PL decay curves recorded at 298 K and under vacuum atmosphere of BN-DBC in toluene solution (1 \times 10 $^{-5}$ M) (a) and with 1 wt% doping concentration in PMMA deposited film (b).

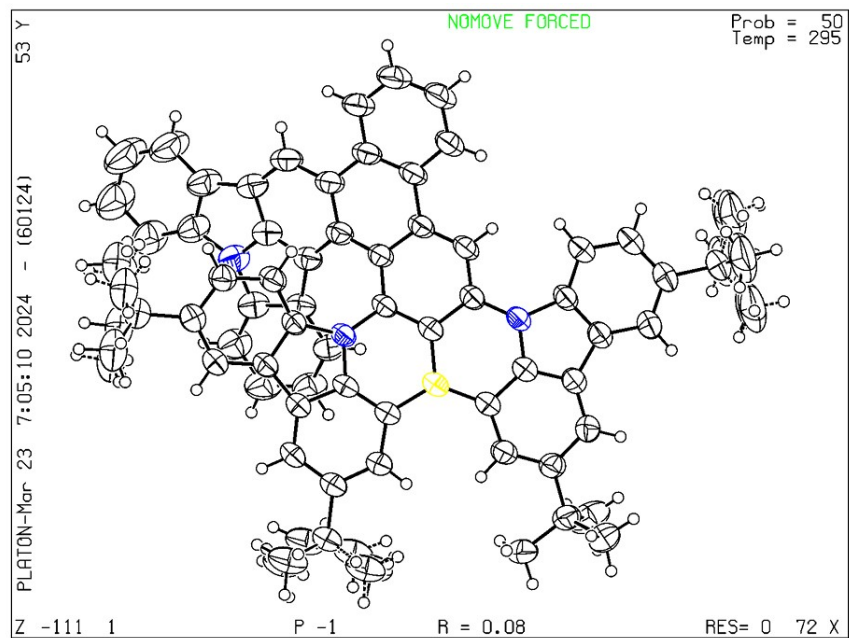


Figure S14. Single crystal structure of BN-TP-ICz (50% probability for thermal ellipsoid).

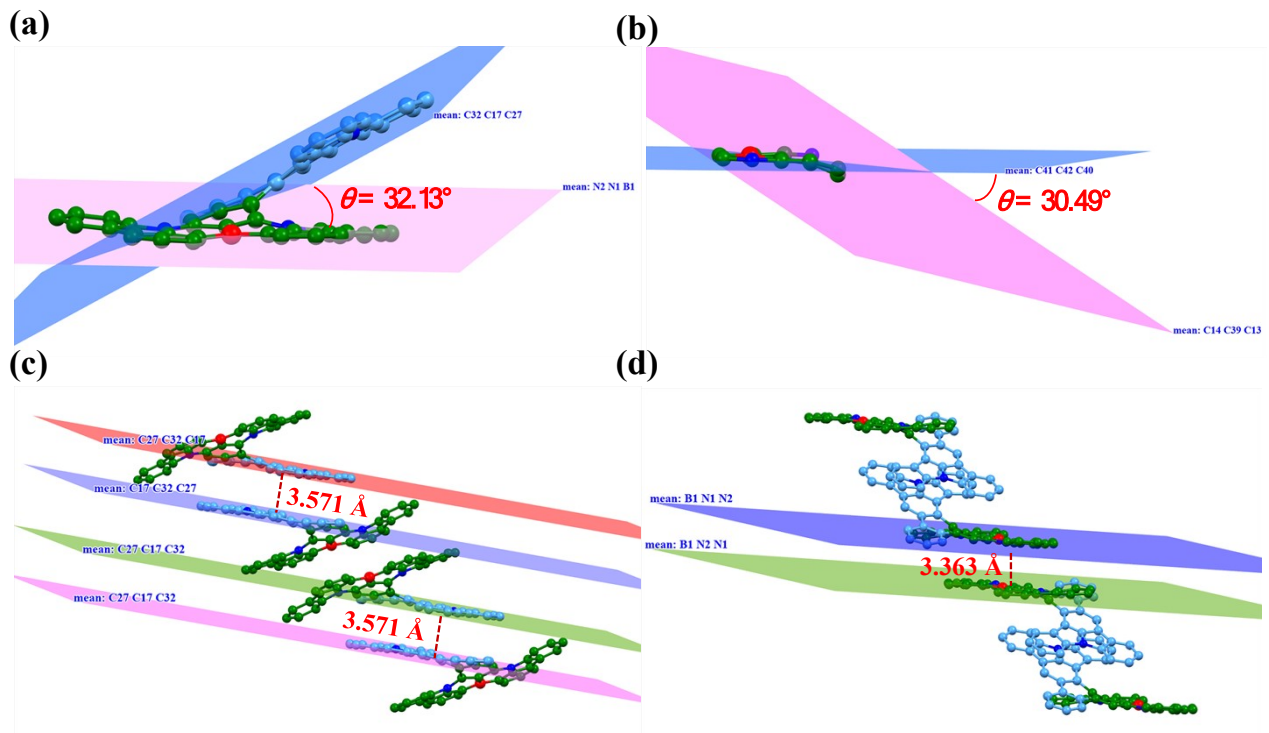


Figure S15. (a) Dihedral angle between the plane where DtCzB moiety lies and the plane where indolo[3,2,1-*j**k*]carbazole (ICz) moiety lies. (b) Torsion angle of the N–B–N-substituted central phenyl ring in DtCzB. (c) $\pi\cdots\pi$ interactions between ICz planes. (d) $\pi\cdots\pi$ interactions between DtCzB planes.

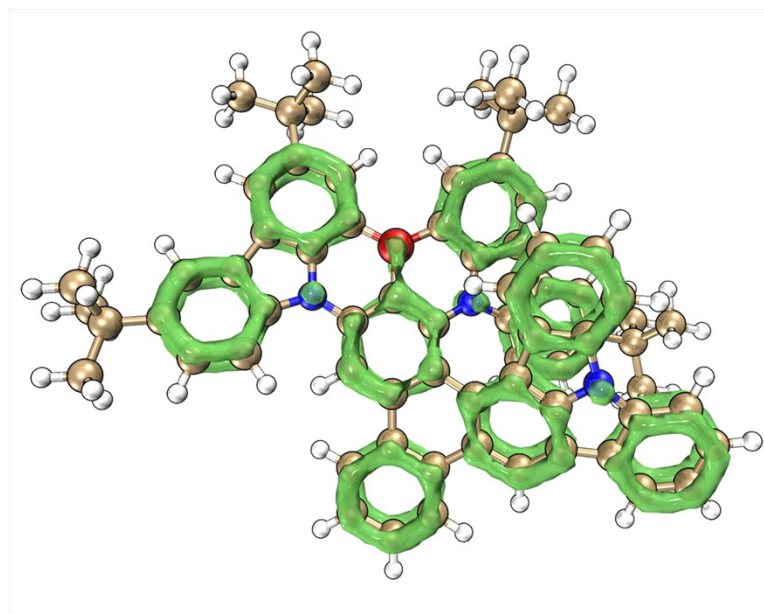


Figure S16. LOL- π isosurface of (P)-BN-TP-ICz (isovalue = 0.5).

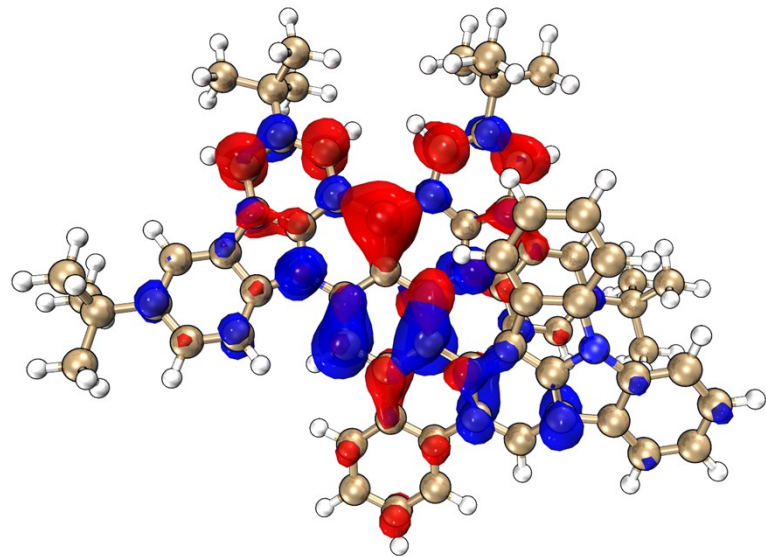


Figure S17. Hole (blue) and electron (red) distribution in S_1 state of (*P*)-BN-TP-ICz.

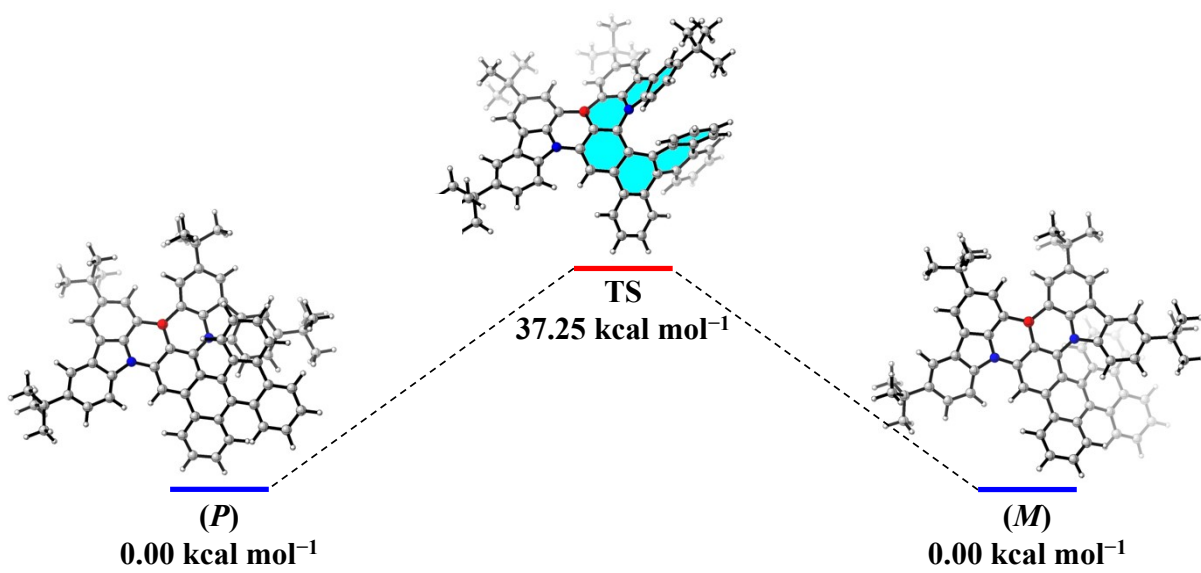


Figure S18. Energy barrier of racemization of enantiomers (*P/M*)-BN-DBC.

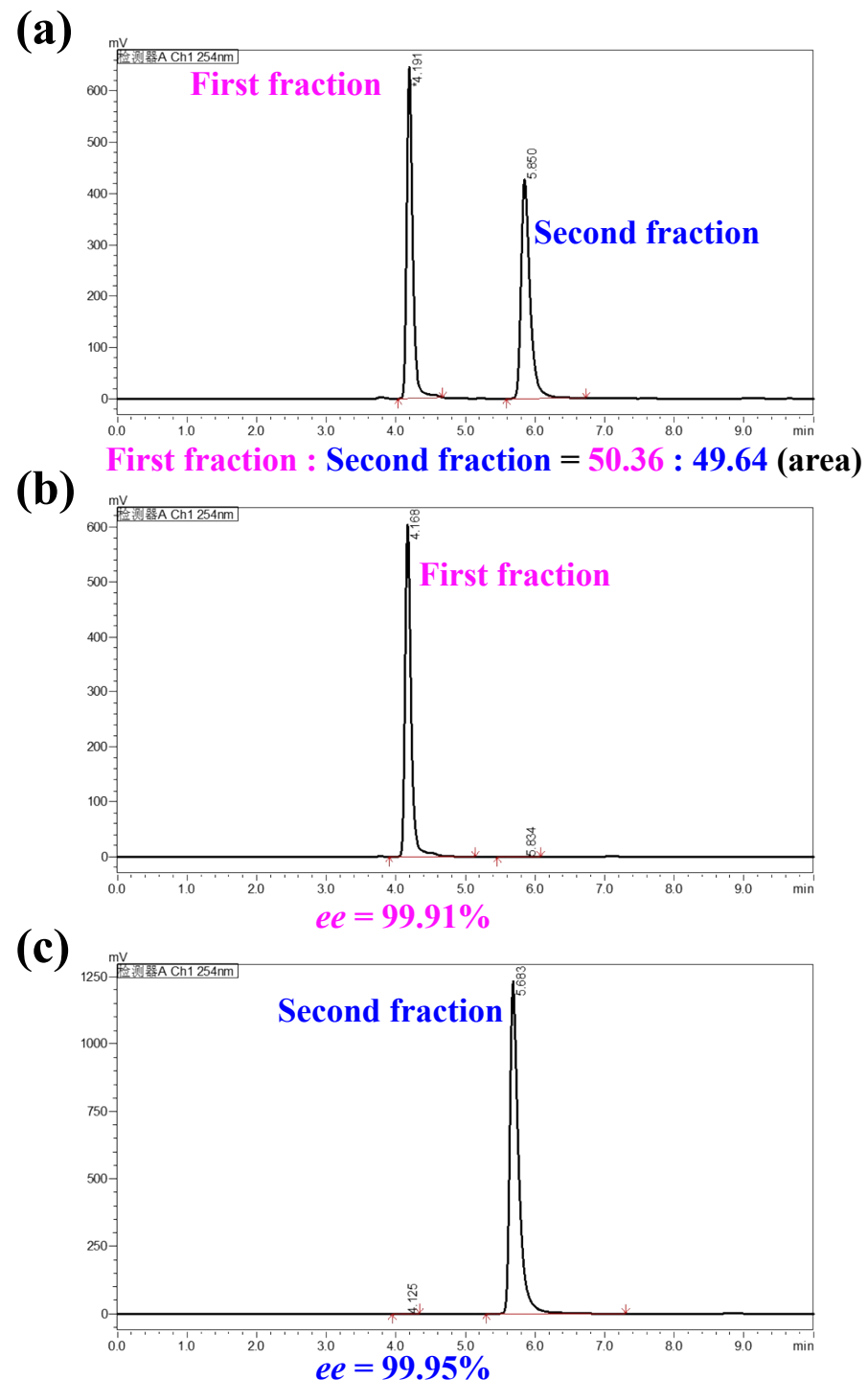


Figure S19. Chiral HPLC analysis of racemic BN-TP-ICz (a) and enantiomer (b) and (c) (Mobile phase: dichloromethane: hexane = 1:1 (a, b) or dichloromethane: ethyl acetate = 19:1 (c), Flow rate: 1.0 mL/min).

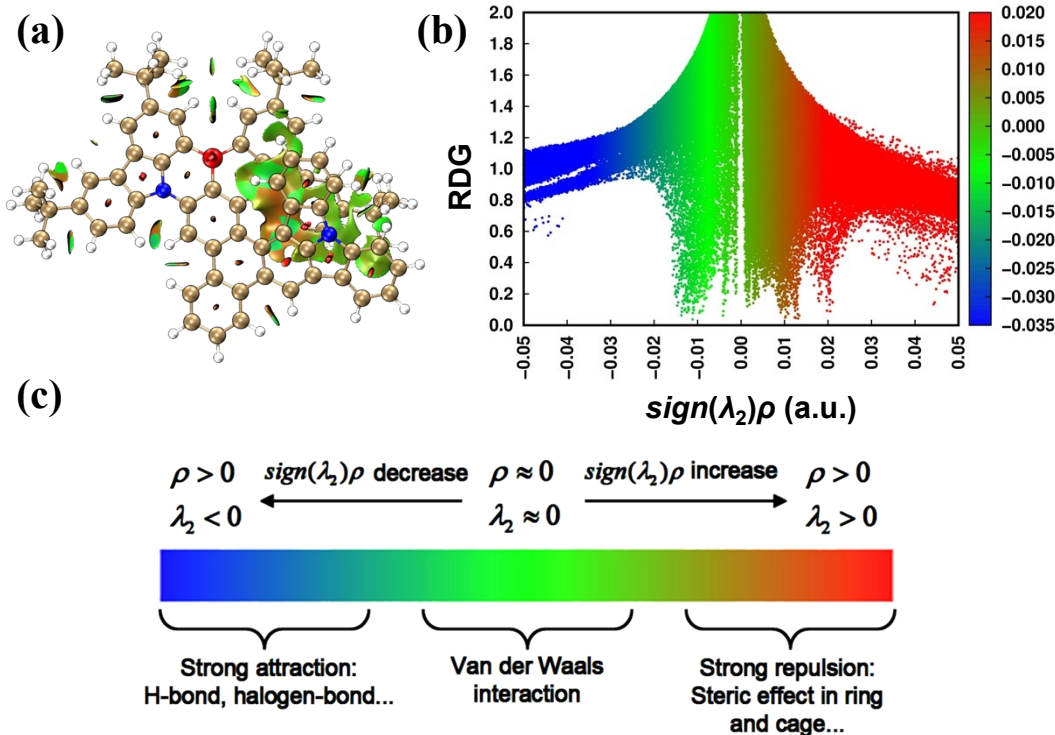


Figure S20. (a) Calculated reduced density gradient isosurface based on optimized S_0 geometry of (P)-BN-TP-ICz. (b) Scattering diagram. (c) Standard coloring method and chemical explanation of $\text{sign}(\lambda_2)\rho$ on RDG isosurface.

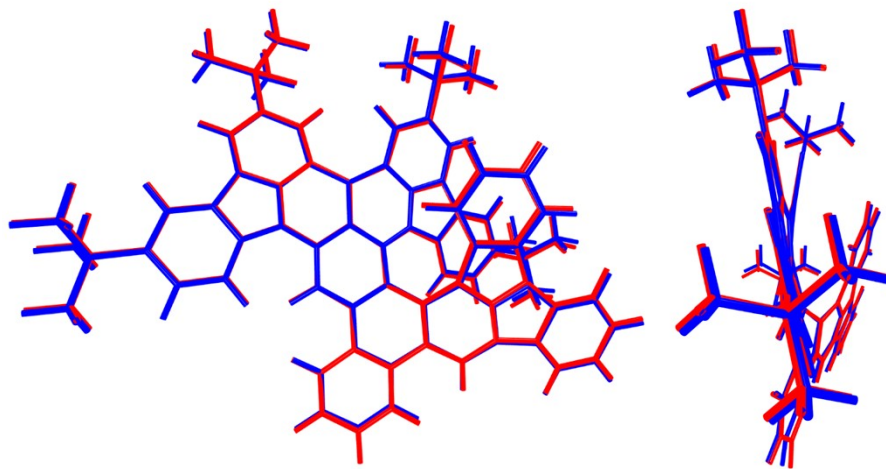


Figure S21. Comparison of the optimized structures of (P)-BN-TP-ICz in S₀ (blue) and S₁ (red).

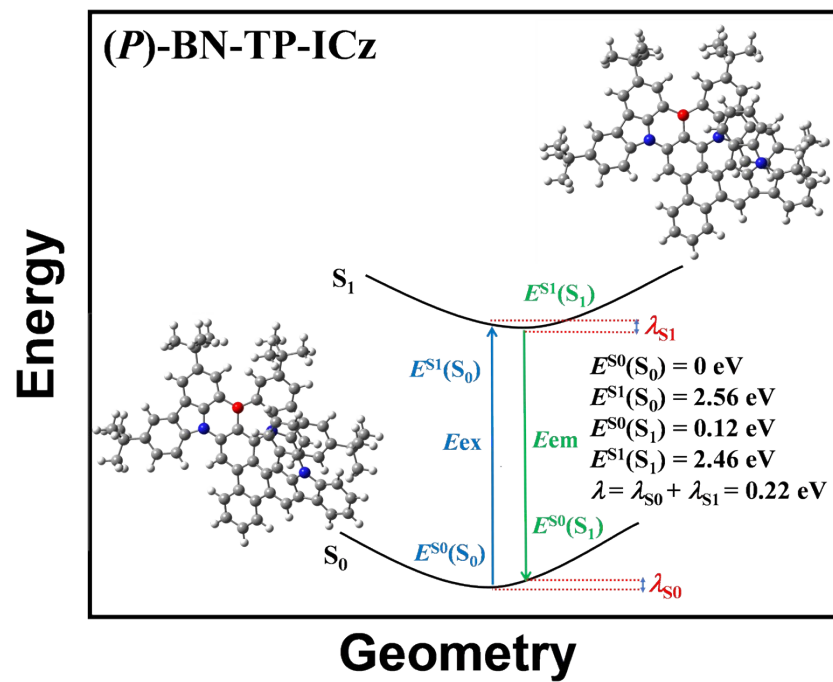


Figure S22. Optimized S₀ and S₁ structures, single point energy, and reorganization energy (λ) of (P)-BN-TP-ICz.

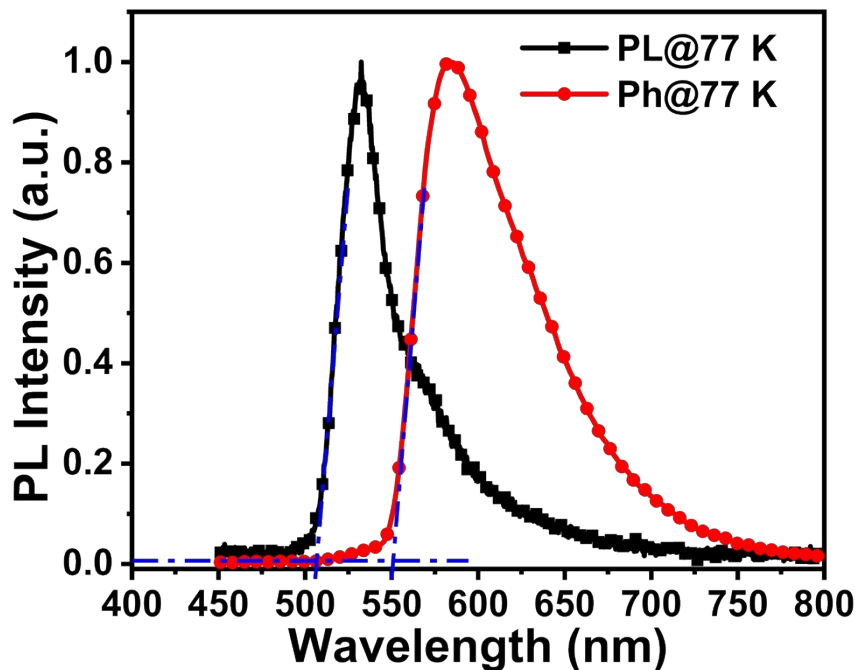


Figure S23. Normalized fluorescence and phosphorescence spectra of BN-TP-ICz measured in toluene solution (1×10^{-5} M, 77 K).

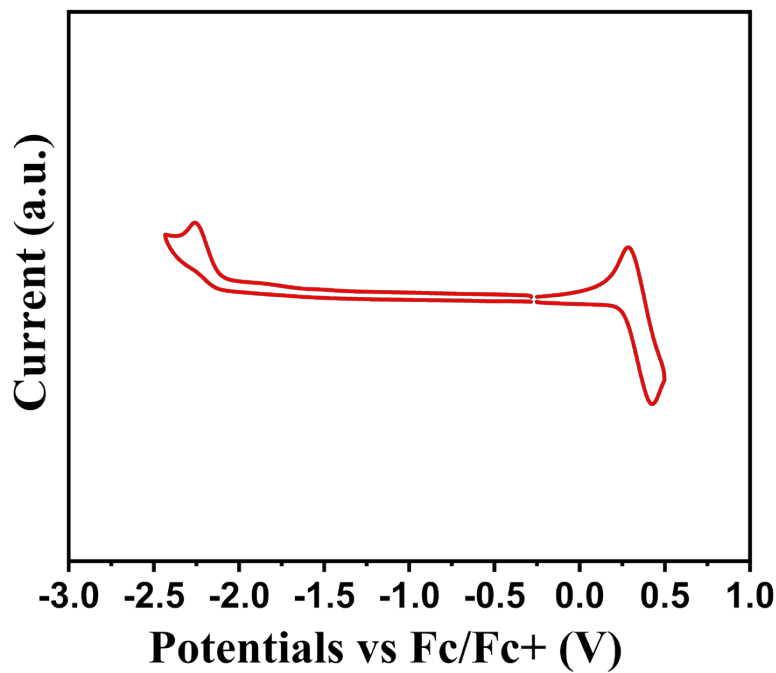


Figure S24. CV curve of BN-TP-ICz.

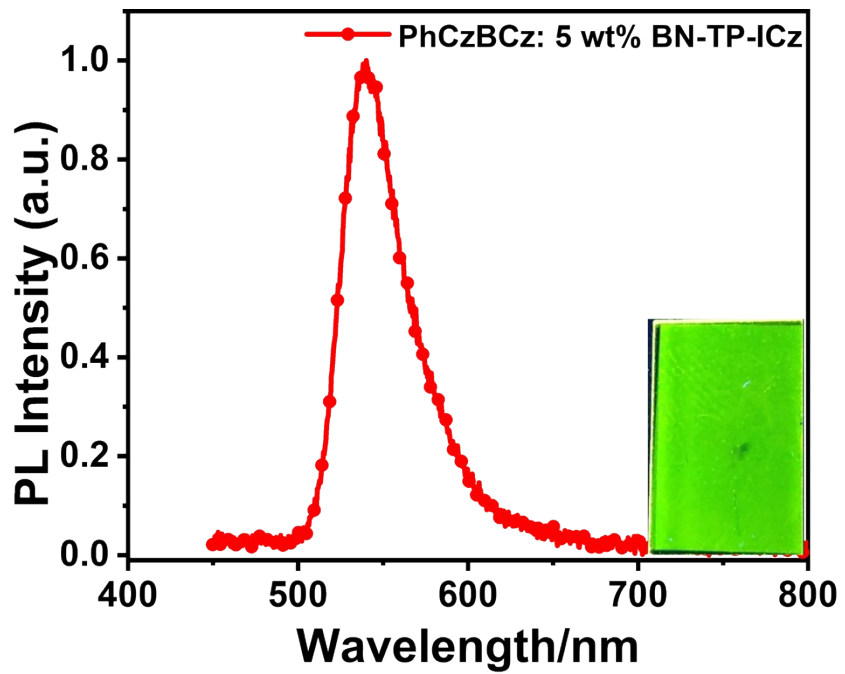


Figure S25. PL spectrum of BN-TP-ICz with 5 wt% doping concentration in PhCzBCz deposited film. (Inset: photograph taken under 365 nm UV light).

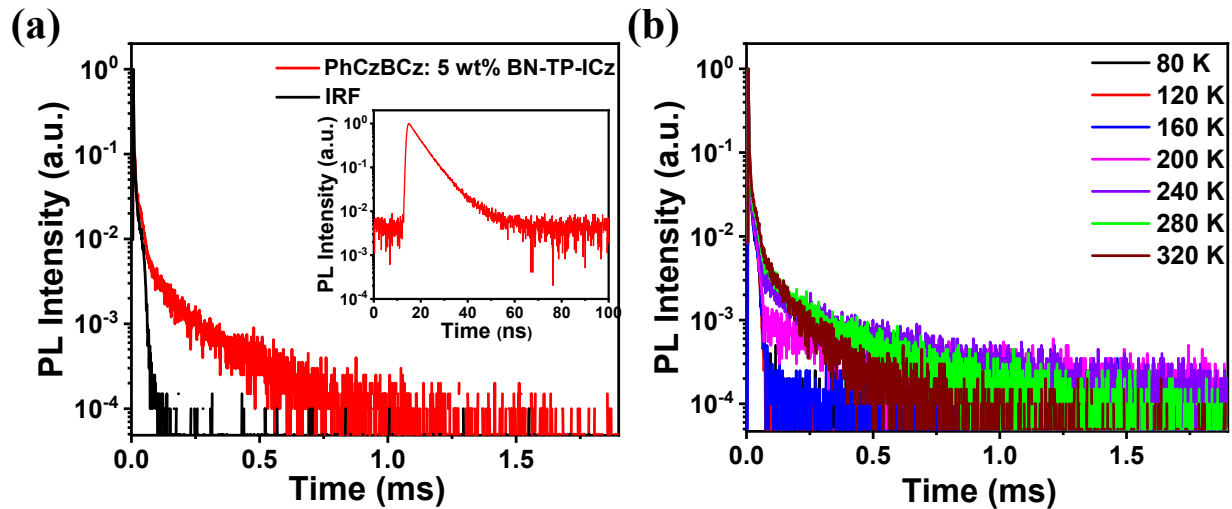


Figure S26. Transient PL decay curve recorded at 298 K and under vacuum (a) and variable-temperature transient PL decay curve (b) of BN-TP-ICz with 5 wt% doping concentration in PhCzBCz deposited film.

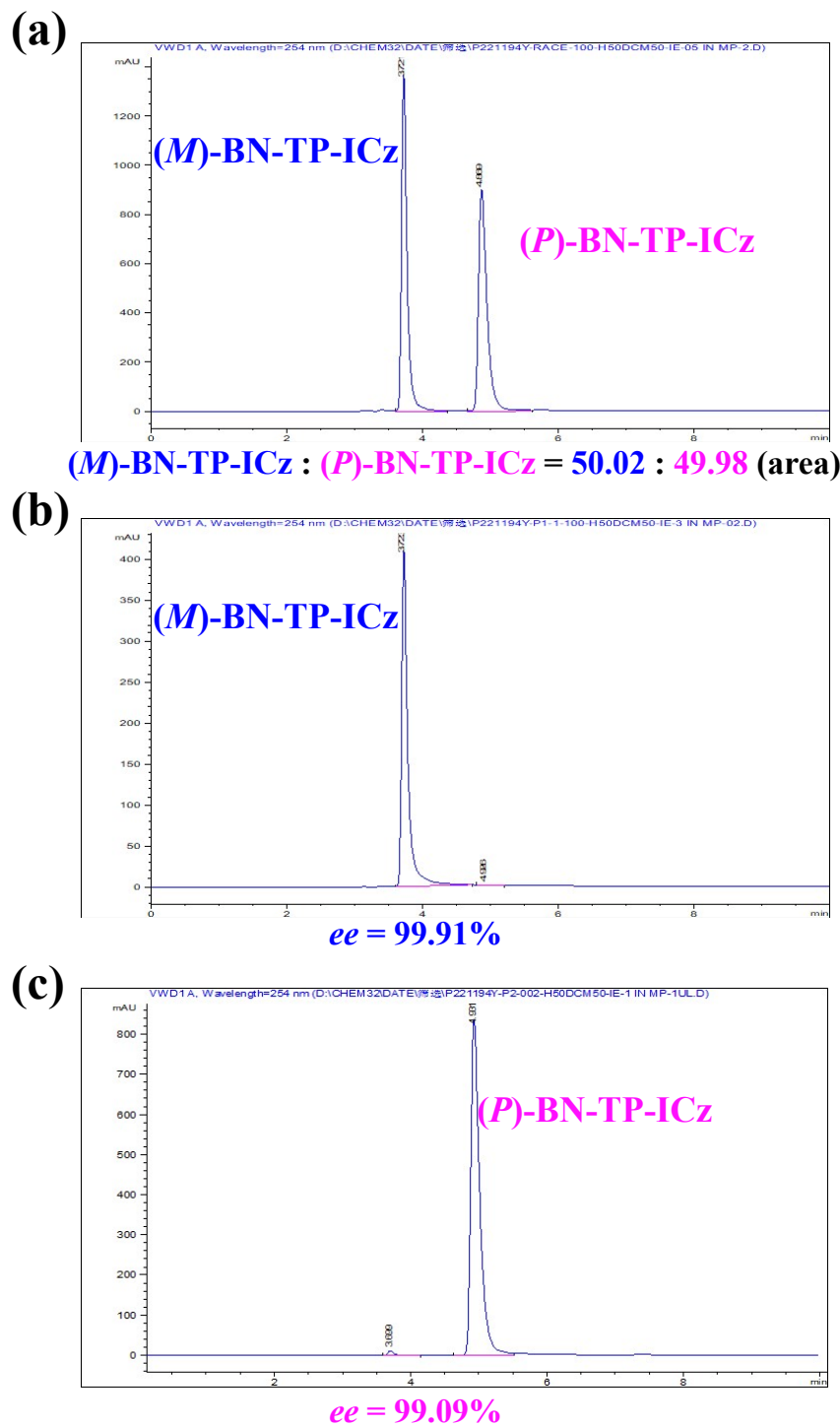


Figure S27. Chiral HPLC analysis of racemic BN-TP-ICz (a) and the residue samples: (M)-BN-TP-ICz (b) and (P)-BN-TP-ICz (c) (Mobile phase: dichloromethane: hexane = 1:1, Flow rate: 1.0 mL/min).

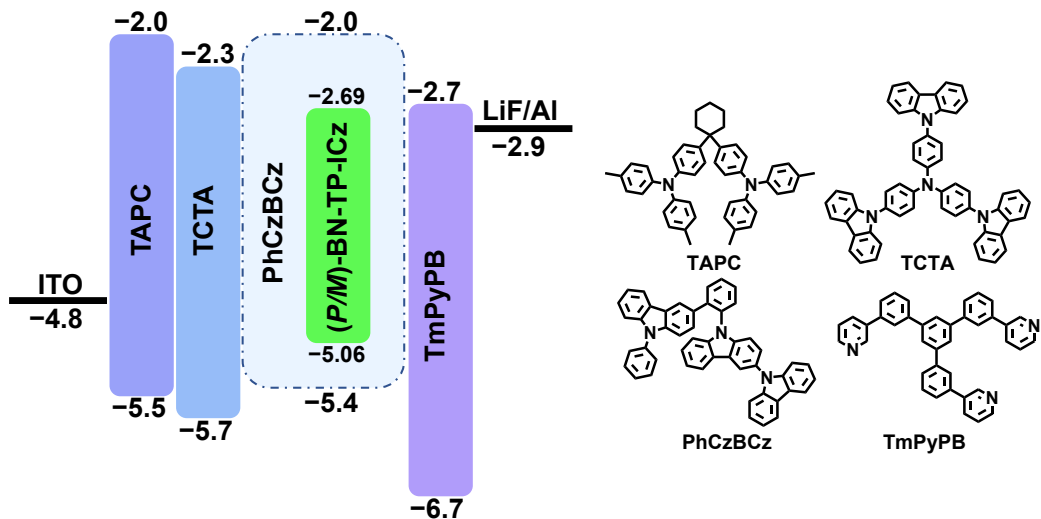


Figure S28. Energy level diagram of the OLEDs and structures of the materials used in the devices with single host.

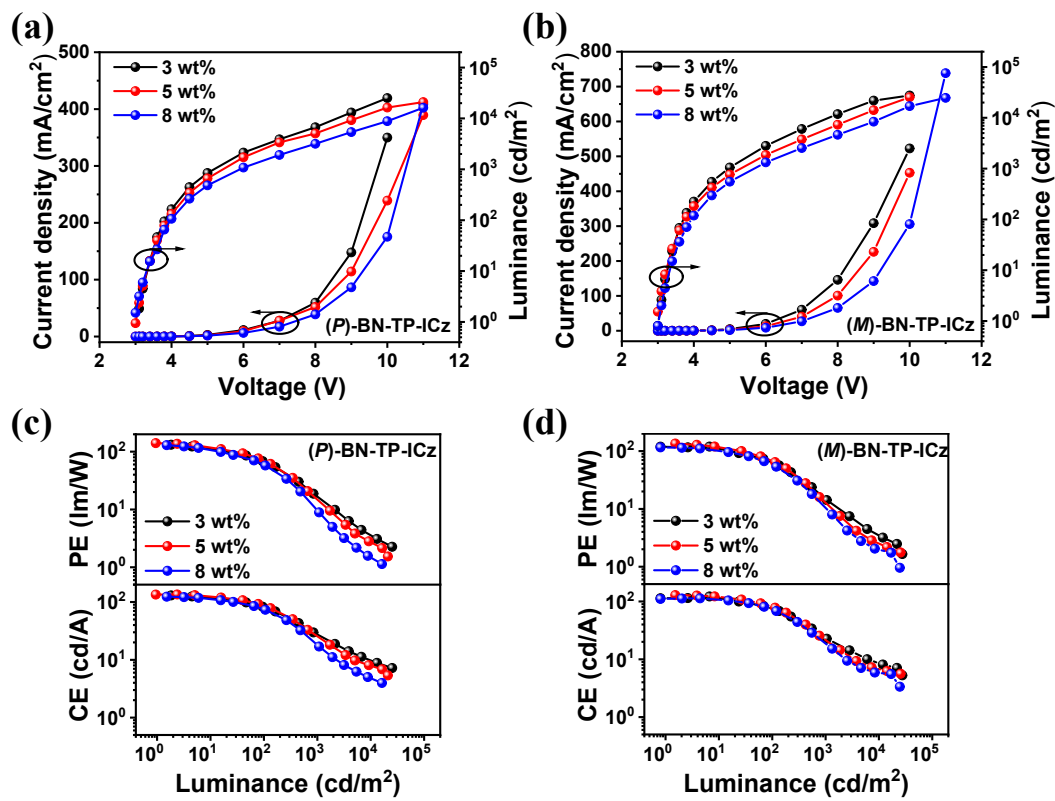


Figure S29. J - V - L curves (a, b), CE- L and PE- L curves (c, d) of the devices with the configuration of [ITO/TAPC (50 nm)/TCTA (5 nm)/PhCzBCz: x wt% (P/M)-BN-TP-ICz (30 nm)/TmPyPB (30 nm)/LiF (1 nm)/Al (100 nm) ($x = 3, 5, 8$)]

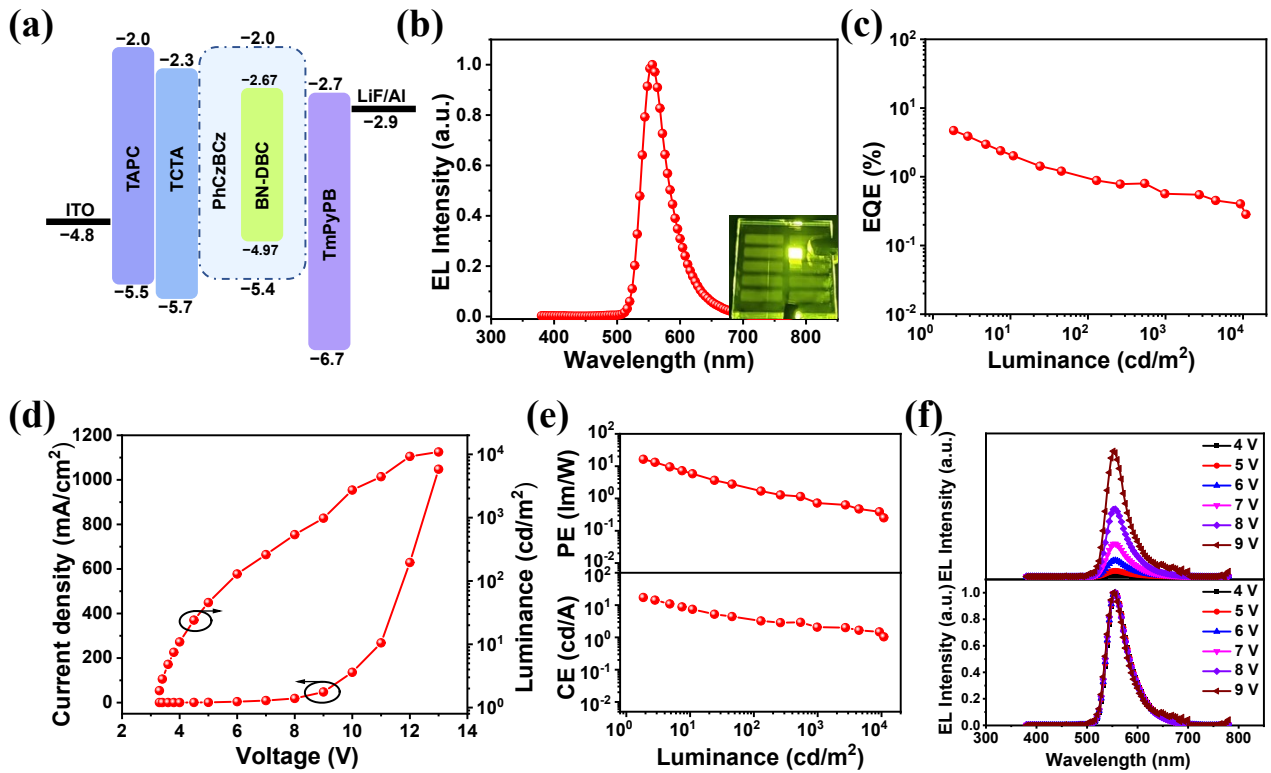


Figure S30. Energy level diagram of the OLED (a), EL spectrum (b), EQE– L curve (c), J – V – L curve (d), CE– L and PE– L curve (e), original (top) and normalized (bottom) EL spectra operated at different voltages (f) of the devices with the configuration of [ITO/TAPC (50 nm)/TCTA (5 nm)/PhCzBCz: 5 wt% BN-DBC (30 nm)/TmPyPB (30 nm)/LiF (1 nm)/Al (100 nm)]. (Inset: photograph showing the emission color of the device with 5 wt% doping concentration).

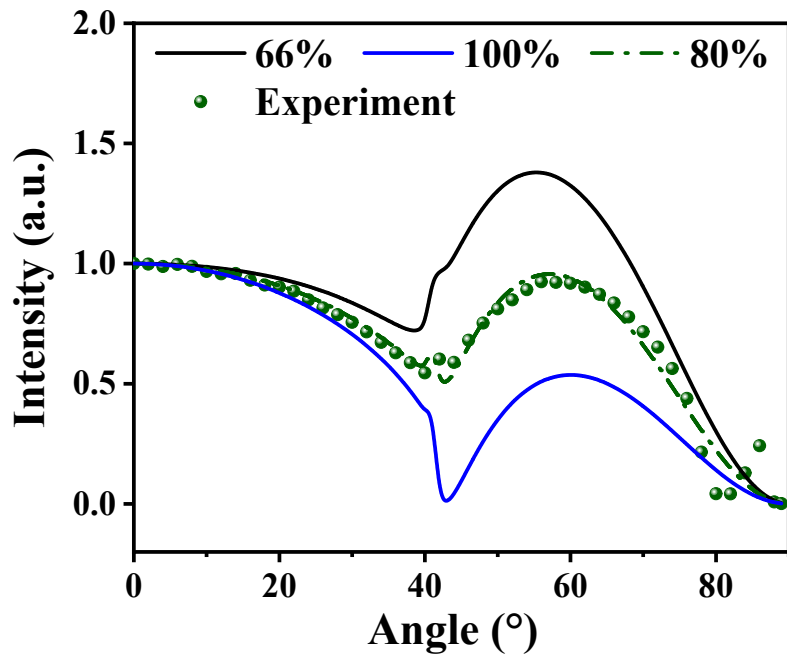


Figure S31. Angel-dependent *p*-polarized PL intensity of EML PhCzBCz: 5 wt% (*P*)-BN-TP-ICz. ($\Theta_{//}$ = 66% denotes isotropic emitting dipole orientation, $\Theta_{//}$ = 100% denotes completely horizontal emitting dipole orientation)

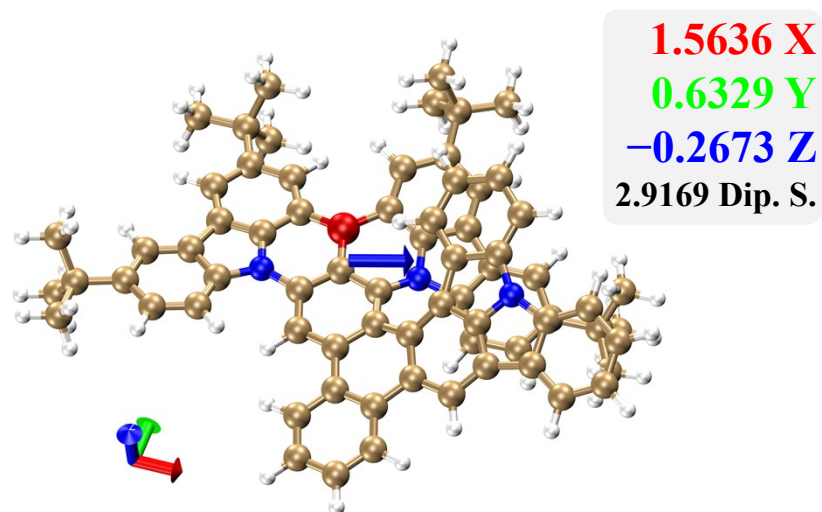


Figure S32. TDM direction and TDM vector ($S_0 \rightarrow S_1$) for (*P*)-BN-TP-ICz relative to the coordinate of molecular structure.

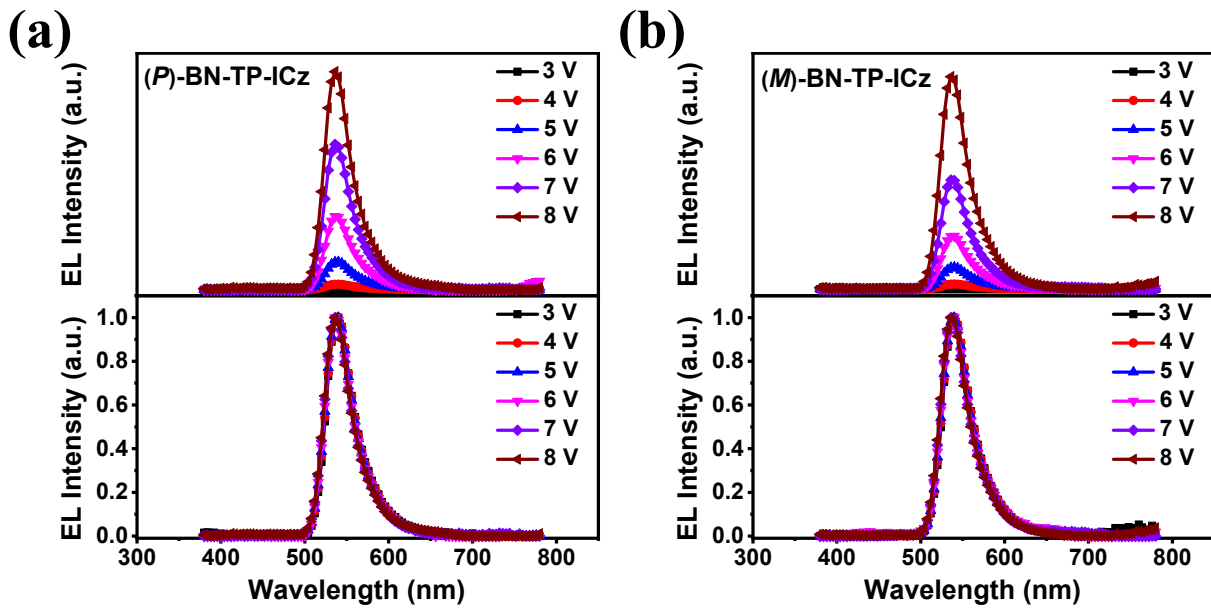


Figure S33. Original (top) and normalized (bottom) EL spectra operated at different voltages of device with the configuration of [ITO/TAPC (50 nm)/TCTA (5 nm)/PhCzBCz: 5 wt% (*P/M*)-BN-TP-ICz (30 nm)/TmPyPB (30 nm)/LiF (1 nm)/Al (100 nm)].

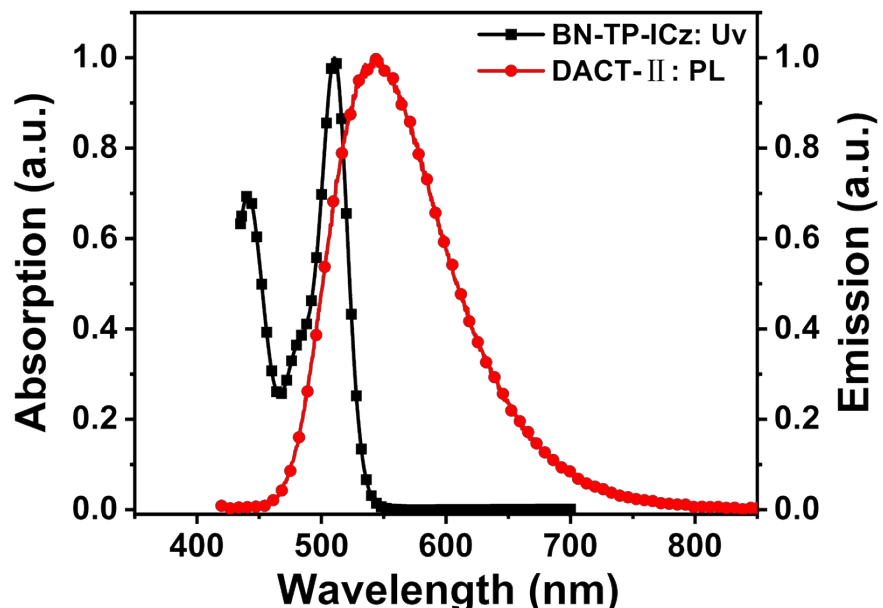


Figure S34. UV-vis absorption spectrum of BN-TP-ICz and PL spectrum of DACT-II measured in toluene solution (1×10^{-5} M, 298 K).

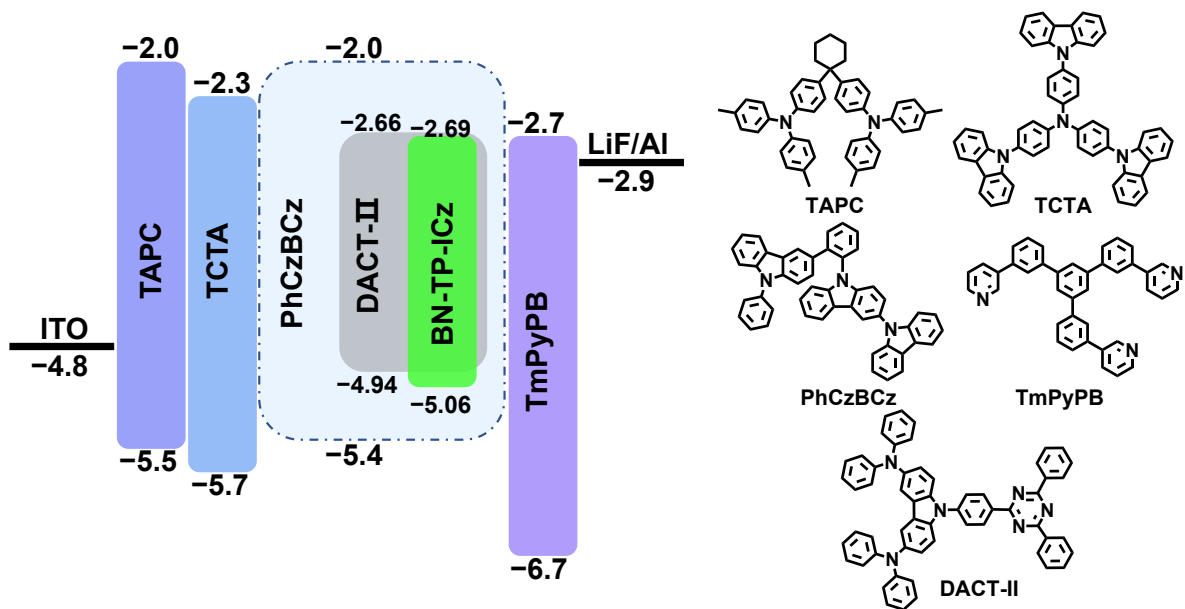


Figure S35. Energy level diagram of the OLEDs and structures of the materials used in the sensitized devices.

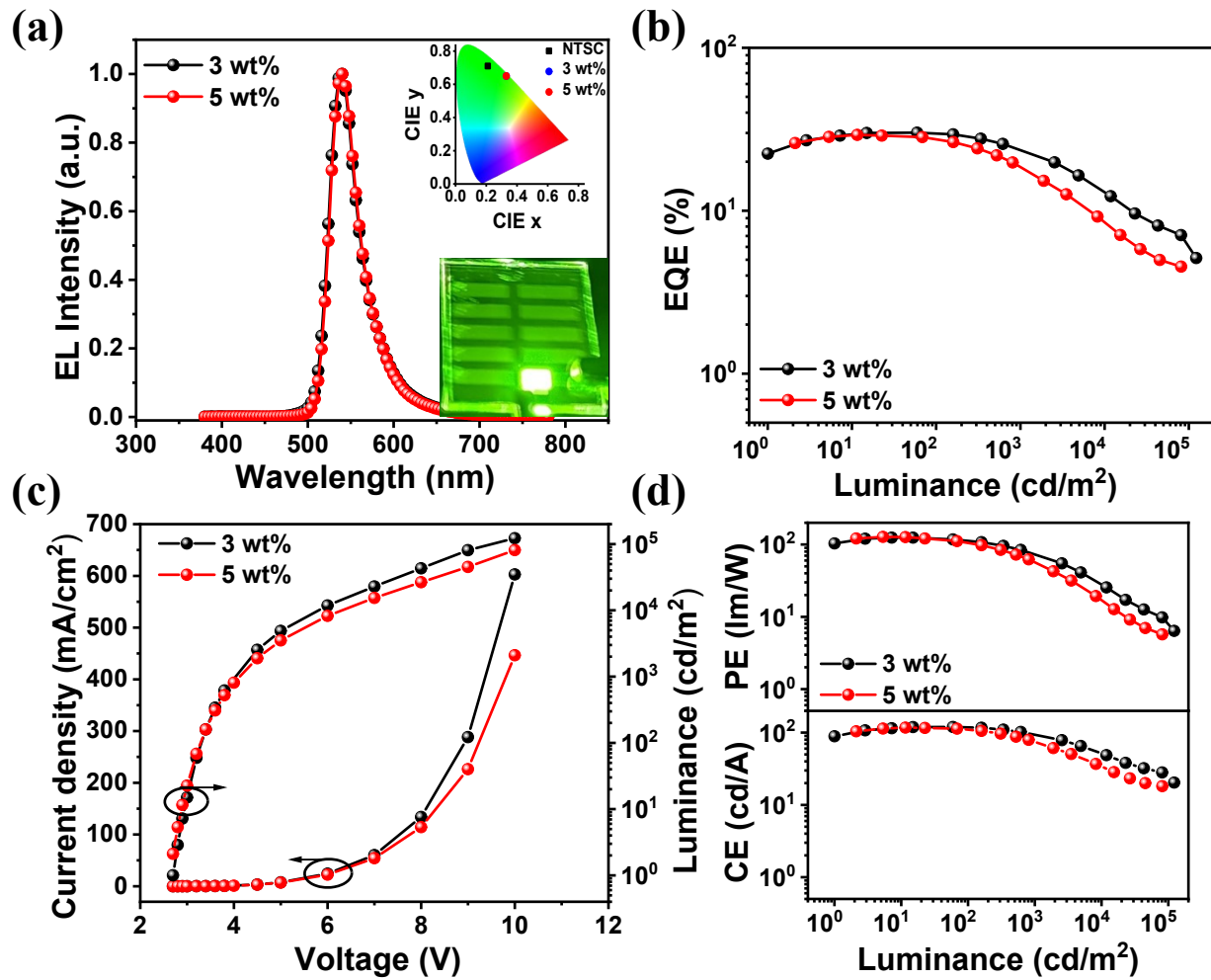


Figure S36. EL spectra (a), EQE– L curves (b), J – V – L curves (c), CE– L and PE– L curves (d) of the devices with the configuration of [ITO/TAPC (50 nm)/TCTA (5 nm)/PhCzBCz: 25 wt% DACT-II: x wt% BN-TP-ICz (30 nm)/TmPyPB (30 nm)/LiF (1 nm)/Al (100 nm) ($x = 3, 5$)]. (Inset: color coordinates of the devices on the CIE 1931 color space, and photograph showing the emission color of the device with 3 wt% doping concentration).

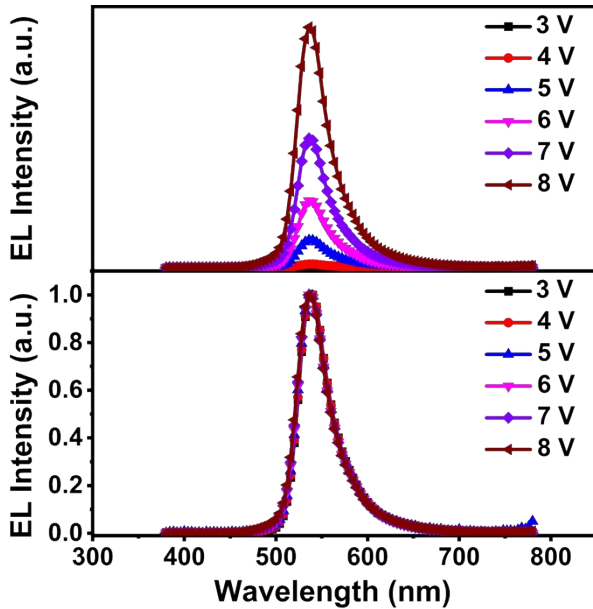


Figure S37. Original (top) and normalized (bottom) EL spectra operated at different voltages of device with the configuration of [ITO/TAPC (50 nm)/TCTA (5 nm)/PhCzBCz: 25 wt% DACT-II : 3 wt% BN-TP-ICz (30 nm)/TmPyPB (30 nm)/LiF (1 nm)/Al (100 nm)].

Although the single host-based devices based on emitters (*P/M*)-BN-TP-ICz exhibit excellent EQE, the efficiency drops seriously. At the optimal 5 wt% doping concentration, the efficiency roll-off at 1000 cd m^{-2} reaches 80.9% and 83.4%, respectively. The main reason for the substantial decrease in efficiency may be attributed to the long duration of the delayed fluorescence lifetime (138.5 μs) of BN-TP-ICz, leading to severe bimolecular collisions at high brightness and subsequent triplet-triplet annihilation or triplet-polaron quenching. And the subsidiary reason may be ascribed to the potential fluorescence quenching caused by $\pi\cdots\pi$ stacking in emitter BN-TP-ICz. To mitigate the efficiency roll-off, sensitizer DACT-II (9-[4-(4,6-diphenyl-1,3,5-triazin-2-yl)phenyl]-*N,N,N',N'*-tetraphenyl-9*H*-carbazole-3,6-diamine) with near-unity Φ_{PL} of 100% and high k_{RISC} of $6.88 \times 10^4 \text{ s}^{-1}$ was introduced into EML,²² owing to the sufficient spectral overlap between its emission spectrum and the absorption spectrum of BN-TP-ICz (**Figure S34**). As a result, the sensitized OLEDs were fabricated via vacuum thermal deposition with the configuration of [ITO/TAPC (50 nm)/TCTA (5 nm)/PhCzBCz: 25 wt% DACT-II : x wt% BN-TP-ICz (30 nm)/TmPyPB (30 nm)/LiF (1 nm)/Al (100 nm)] (**Figure S35**). The EL spectra, EQE–*L* curves,

J–*V*–*L* curves, CE–*L* and PE–*L* curves are depicted in **Figure S36**, and the detailed EL performance parameters are listed in **Table S5**.

Compared to single host-based devices, the sensitized devices exhibit lower turn-on voltages (≤ 2.8 V), signifying that the introduction of DACT-II improves carrier injection and transport capabilities. The sensitized device exhibits the best EL performances at 3 wt% doping concentration of BN-TP-ICz, showing green emission with a peak of 540 nm and a FWHM of 39 nm, and CIE coordinates of (0.33, 0.65), and has maximum EQE of 30.1%, maximum CE of 119.6 cd A $^{-1}$, and maximum PE of 124.7 lm W $^{-1}$. The involvement of DACT-II also significantly improves the maximum luminance of device, reaching 122,600 cd m $^{-2}$, and considerably alleviates the efficiency roll-off at 1000 cd m $^{-2}$, which drops 21.9%. This indicates that DACT-II promotes the up-conversion of triplet excitons and improves exciton utilization. Furthermore, the device demonstrates good spectral stability within the operating voltage range of 3–8 V (**Figure S37**), indicating efficient energy transfer and stable exciton recombination regions within the device.

Table S1. Summary of PL spectra data of BN-DBC in toluene solution and with 1 wt% doping concentration in PMMA deposited film.

State	$\lambda_{\text{abs}}^{\text{a})}$ [nm]	$\lambda_{\text{em}}^{\text{b})}$ [nm]	FWHM ^{c)} [nm]	$E_{S1}^{\text{d})}$ [eV]	$E_{T1}^{\text{e})}$ [eV]	$\Delta E_{ST}^{\text{f})}$ [eV]	$E_g^{\text{g})}$ [eV]	$\Phi_{PL}^{\text{h})}$ [%]	$\tau_F^{\text{i})}$ [ns]
Solution	519	548	44	2.40	2.08	0.32	2.28	55	6.2
Film	–	553	50	2.33	2.02	0.31	–	60	6.6

^{a)} Peak wavelength of the lowest energy absorption band. ^{b)} Peak wavelength of the PL spectrum in toluene (1×10^{-5} M, 298 K). ^{c)} Full width at half maximum. ^{d)} Singlet energy estimated from the onset of the fluorescence spectrum in toluene (1×10^{-5} M, 77 K). ^{e)} Triplet energy estimated from the onset of the phosphorescence spectrum in a frozen toluene matrix (1×10^{-5} M, 77 K). ^{f)} $\Delta E_{ST} = E_{S1} - E_{T1}$. ^{g)} Optical band gap estimated from the absorption edge of the UV-vis spectrum. ^{h)} Absolute photoluminescence quantum yield measured with an integer-sphere system in N₂-bubbling toluene. ⁱ⁾ The lifetime of prompt fluorescence (τ_F).

Table S2. Crystal data and structure refinement for BN-TP-ICz.

compound	BN-TP-ICz
CCDC number	2361156
Empirical formula	C ₇₀ H ₆₀ BN ₃
Formula weight	954.02
Temperature/K	295.0
Crystal system	triclinic
Space group	<i>P</i> 1
a/Å	11.1226(7)
b/Å	15.8329(9)
c/Å	15.9866(9)
α/°	104.893(2)
β/°	90.229(2)
γ/°	96.128(2)
Volume/Å ³	2703.7(3)
Z	2
ρ _{calc} g/cm ³	1.172
μ/mm ⁻¹	0.067
F(000)	1012.0
Crystal size/mm ³	0.13 × 0.12 × 0.1
Radiation	MoKα ($\lambda = 0.71073$)
2θ range for data collection/°	5.06 to 55.06
Index ranges	-14 ≤ h ≤ 14, -20 ≤ k ≤ 20, -20 ≤ l ≤ 20
Reflections collected	113254
Independent reflections	12428 [R _{int} = 0.0709, R _{sigma} = 0.0382]
Data/restraints/parameters	12428/34/682
Goodness-of-fit on F ²	1.028
Final R indexes[I >= 2σ (I)]	R ₁ = 0.0762, wR ₂ = 0.1967
Final R indexes [all data]	R ₁ = 0.1271, wR ₂ = 0.2410
Largest diff. peak/hole / e Å ⁻³	0.60/-0.42

Table S3. Summary of photophysical data of BN-TP-ICz with 5 wt% doping concentration in PhCzBCz deposited film.

compound	BN-TP-ICz
$\Phi_{PL}^a)$ [%]	92
$\Phi_F^b)$ [%]	76.4
$\Phi_{TADF}^c)$ [%]	15.6
$\tau_F^d)$ [ns]	5.8
$Ref_F^e)$ [%]	83.0
$\tau_{TADF}^f)$ [μ s]	138.5
$Ref_{TADF}^g)$ [%]	17.0
$k_F^h)$ [10^7 s $^{-1}$]	13.2
$k_{IC}^i)$ [10^7 s $^{-1}$]	1.15
$k_{ISC}^j)$ [10^7 s $^{-1}$]	2.92
$k_{TADF}^k)$ [10^4 s $^{-1}$]	0.66
$k_{RISC}^l)$ [10^4 s $^{-1}$]	0.61
$\Phi_{ISC}^m)$ [%]	17.0

^{a)} The total photoluminescence quantum yield (Φ_{PL}). ^{b)} The prompt fluorescent (Φ_F) component of Φ_{PL} . ^{c)} The delayed fluorescent (Φ_{TADF}) component of Φ_{PL} . ^{d)} The lifetime of prompt fluorescence (τ_F). ^{e)} The proportion of prompt fluorescence lifetime. ^{f)} The lifetime of delayed fluorescence (τ_{TADF}). ^{g)} The proportion of delayed fluorescence lifetime. ^{h)} The rate constant of prompt fluorescence (k_F). ⁱ⁾ The rate constant of internal conversion (k_{IC} : S₁ \rightarrow S₀). ^{j)} The rate constant of intersystem crossing (k_{ISC}). ^{k)} The rate constant of TADF (k_{TADF}). ^{l)} The rate constant of reverse intersystem crossing (k_{RISC}). ^{m)} The efficiency of ISC (Φ_{ISC}).

Table S4. Summary of EL data of device (single host: PhCzBCz) based on emitter BN-DBC with 5**Table S6.** Summary of B_{CPL} of representative single-helicene-based CPL emitters.

Emitter	$\epsilon / (\text{M}^{-1} \cdot \text{cm}^{-1})$ ($\lambda_{\text{abs}} / \text{nm}$)	Φ ($\lambda_{\text{em}} / \text{nm}$)	$g_{\text{lum}} \times 10^3$	$B_{\text{CPL}} /$ ($\text{M}^{-1} \cdot \text{cm}^{-1}$)	Reference
(P)-BN-TP-ICz	32136 (510)	0.93 (531)	0.53	8.6	This work
[5]Helicene					
Hel-1	9332 (414)	0.22 (518)	0.9	0.9	23
Hel-2	7400 (420)	0.30 (502)	0.95	1.1	24
Hel-3	2500 (444)	0.19 (558)	6.5	1.5	25

wt% doping concentration.

x wt%	$\lambda_{\text{em}}^{\text{a})}$ [nm]	FWHM ^{b)} [nm]	CIE(x, y) ^{c)}	$V_{\text{on}}^{\text{d})}$ [V]	$L_{\text{max}}^{\text{e})}$ [cd m ⁻²]	$\text{CE}_{\text{max}}^{\text{f})}$ [cd A ⁻¹]	$\text{PE}_{\text{max}}^{\text{g})}$ [lm W ⁻¹]	EQE ^{h)} [%]
5	556	47	(0.43, 0.57)	3.3	10890	17.2	16.4	4.7/1.0/0.6

^{a)} EL peak wavelength. ^{b)} Full-width at half-maximum. ^{c)} Commission Internationale de L'Eclairage coordinates (value taken at 100 cd m⁻²). ^{d)} Turn-on voltage at 1 cd m⁻². ^{e)} Maximum luminance. ^{f)} Maximum current efficiency. ^{g)} Maximum power efficiency. ^{h)} Maximum external quantum efficiency, and values at 100 and 1000 cd m⁻², respectively.

Table S5. Summary of EL data of devices (single host: PhCzBCz, sensitizer: DACT-II) based on emitter BN-TP-ICz with different doping concentration.

x wt%	$\lambda_{\text{em}}^{\text{a})}$ [nm]	FWHM ^{b)} [nm]	CIE(x, y) ^{c)}	$V_{\text{on}}^{\text{d})}$ [V]	$L_{\text{max}}^{\text{e})}$ [cd m ⁻²]	$\text{CE}_{\text{max}}^{\text{f})}$ [cd A ⁻¹]	$\text{PE}_{\text{max}}^{\text{g})}$ [lm W ⁻¹]	EQE ^{h)} [%]
3	540	39	(0.33, 0.65)	2.7	122600	119.6	124.7	30.1/29.7/23.5
5	540	39	(0.33, 0.65)	2.7	81180	117.0	127.6	29.2/27.4/18.5

^{a)} EL peak wavelength. ^{b)} Full-width at half-maximum. ^{c)} Commission Internationale de L'Eclairage coordinates (value taken at 100 cd m⁻²). ^{d)} Turn-on voltage at 1 cd m⁻². ^{e)} Maximum luminance. ^{f)} Maximum current efficiency. ^{g)} Maximum power efficiency. ^{h)} Maximum external quantum efficiency, and values at 100 and 1000 cd m⁻², respectively.

Hel-4	51000 (330)	0.19 (455)	0.35	1.7	26
Hel-5	1100 (422)	0.51 (445)	6.3	1.8	25
Hel-6	55000 (301)	0.39 (425)	0.42	4.5	26
Hel-7	55000 (305)	0.27 (408)	0.76	5.6	27
Hel-8	32000 (320)	0.22 (500)	2.3	8.1	28
Hel-9	98000 (320)	0.35 (406)	0.61	10.5	27
Hel-10	28000 (330)	0.37 (460)	2.4	12.4	28
[6]Helicene					
Hel-11	21000 (310)	0.03 (430)	0.8	0.2	29
Hel-12	35000 (580)	0.41 (610)	0.1	0.7	30
Hel-13	30400 (307)	0.21 (430)	0.9	2.9	31
Hel-14	34000 (320)	0.08 (421)	3.2	4.3	32, 33
Hel-15	15000 (332)	0.05 (437)	25	9.4	34, 35
Hel-16	18100 (342)	0.49 (430)	2.3	10.2	31
Hel-17	85000 (580)	0.41 (610)	0.6	10.5	30
Hel-18	41000 (420)	0.70 (436)	3.2	45.9	36
Hel-19	72000 (420)	0.45 (436)	9.5	153.9	36
[7]Helicene					
Hel-20	25500 (324)	0.07 (442)	0.7	0.6	31
Hel-21	20000 (325)	0.25 (560)	0.4	1	37
Hel-22	37200 (317)	0.10 (449)	0.8	1.2	38
Hel-23	17000 (380)	0.23 (473)	0.95	1.9	39
Hel-24	65000 (345)	0.06 (494)	2.2	4.3	40
Hel-25	20000 (300)	0.23 (450)	3.5	8	41
Hel-26	30000 (330)	0.31 (428)	1.9	8.8	42
Hel-27	19000 (320)	0.39 (417)	3	11.1	43
Hel-28	8400 (416)	0.39 (473)	9	14.7	44
Hel-29	28000 (500)	0.36 (560)	3	15.1	45
Hel-30	45000 (500)	0.66 (550)	1.2	17.8	46
Hel-31	17000 (337)	0.58 (456)	7.6	37.6	47

Hel-32	34000 (300)	0.15 (482)	16	40.8	48
Hel-33	9800 (273)	0.30 (449)	32	47	49
Hel-34	10000 (364)	0.32 (428)	30	48	49

[8]Helicene

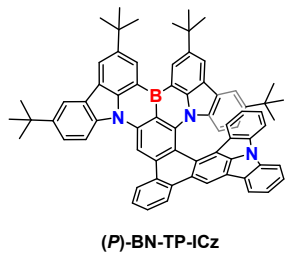
Hel-35	10000 (365)	0.19 (488)	8	7.6	47
--------	-------------	------------	---	-----	----

[9]Helicene

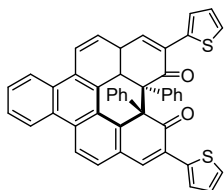
Hel-36	7000 (388)	0.18 (547)	1.1	0.7	39
Hel-37	31200 (337)	0.07 (473)	1	1.1	31
Hel-38	60000 (315)	0.085 (501)	0.48	1.2	50
Hel-39	11000 (355)	0.27 (430)	0.87	1.3	51
Hel-40	21000 (335)	0.16 (492)	20	33.6	47
Hel-41	110000 (400)	0.26 (600)	3	42.9	52

[11]Helicene

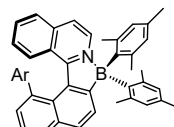
Hel-42	60000 (290)	0.002 (437)	8	0.5	53
Hel-43	40000 (290)	0.014 (420)	8	2.2	53



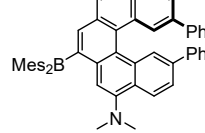
(P)-BN-TP-ICz



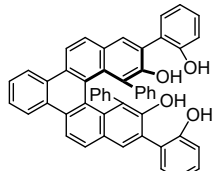
Hel-1



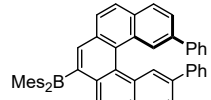
Hel-2 Ar =



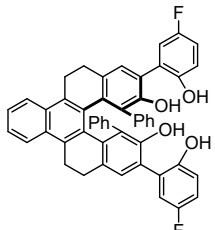
Hel-3



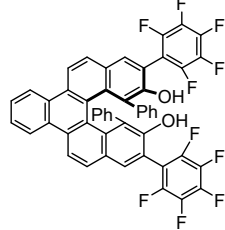
Hel-4



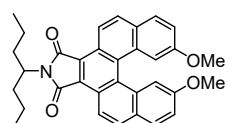
Hel-5



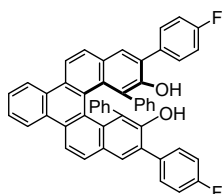
Hel-6



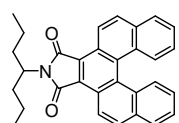
Hel-7



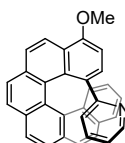
Hel-8



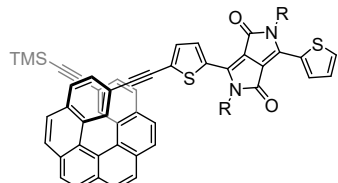
Hel-9



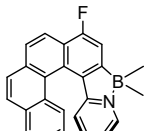
Hel-10



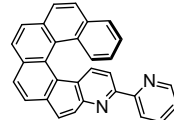
Hel-11



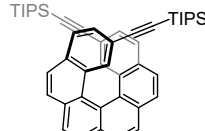
Hel-12 R = octyl



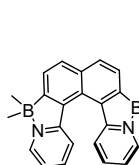
Hel-13



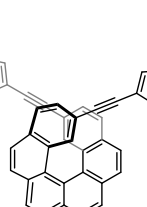
Hel-14



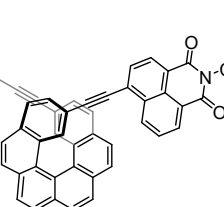
Hel-15



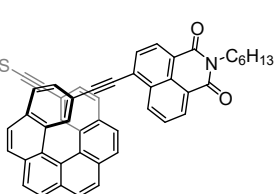
Hel-16



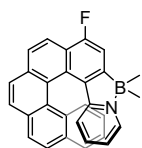
Hel-17 R = octyl



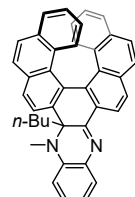
Hel-18



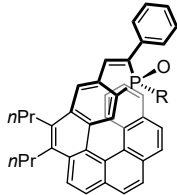
Hel-19



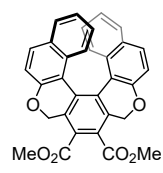
Hel-20



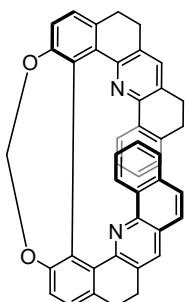
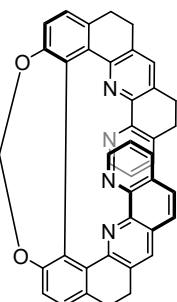
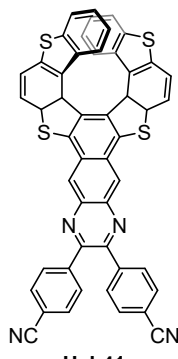
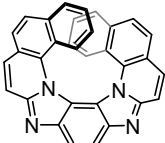
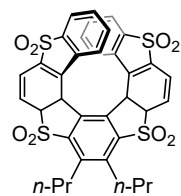
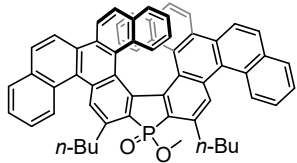
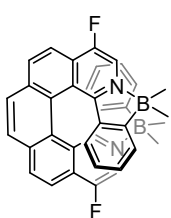
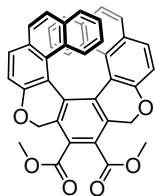
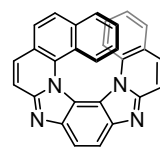
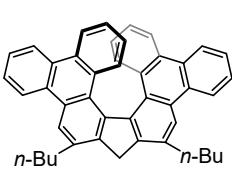
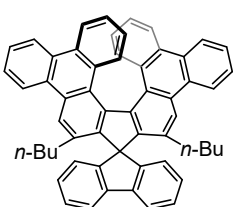
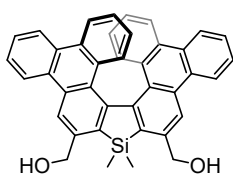
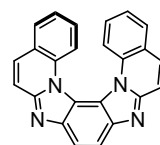
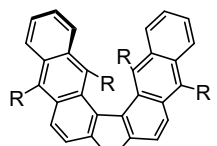
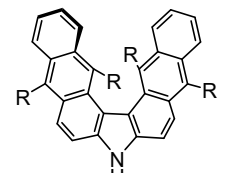
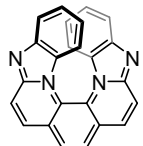
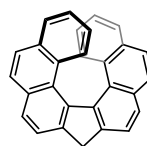
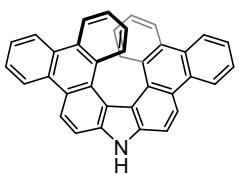
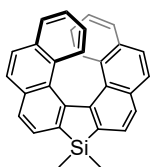
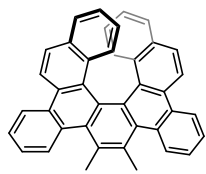
Hel-21



Hel-22 R = l-menthyl



Hel-23



References

- 1 Dolomanov, O.V., Bourhis, L.J., Gildea, R.J., Howard, J.A.K. & Puschmann, H., *J. Appl. Cryst.* **2009**, *42*, 339–341.
- 2 Sheldrick, G.M., *Acta Cryst.* **2015**, *A71*, 3–8.
- 3 Sheldrick, G.M., *Acta Cryst.* **2008**, *A64*, 112–122.
- 4 A. D. Becke, *J. Chem. Phys.* **1993**, *98*, 5648–5652.
- 5 C. Lee, W. Yang, R. G. Parr, *Phys. Rev. B* **1988**, *37*, 785–789.
- 6 R. Krishnan, J. S. Binkley, R. Seeger, J. Pople, *J. Chem. Phys.* **1980**, *72*, 650–654.
- 7 S. Grimme, J. Antony, S. Ehrlich, H. Krieg, *J. Chem. Phys.* **2010**, *132*, 154104.
- 8 Gaussian 09, Revision D.01, M. J. Frisch, G. W. Trucks, H. B. Schlegel, G. E. Scuseria, M. A. Robb, J. R. Cheeseman, G. Scalmani, V. Barone, B. Mennucci, G. A. Petersson, H. Nakatsuji, M. Caricato, X. Li, H. P. Hratchian, A. F. Izmaylov, J. Bloino, G. Zheng, J. L. Sonnenberg, M. Hada, M. Ehara, K. Toyota, R. Fukuda, J. Hasegawa, M. Ishida, T. Nakajima, Y. Honda, O. Kitao, H. Nakai, T. Vreven, J. A. Montgomery, Jr., J. E. Peralta, F. Ogliaro, M. Bearpark, J. J. Heyd, E. Brothers, K. N. Kudin, V. N. Staroverov, T. Keith, R. Kobayashi, J. Normand, K. Raghavachari, A. Rendell, J. C. Burant, S. S. Iyengar, J. Tomasi, M. Cossi, N. Rega, J. M. Millam, M. Klene, J. E. Knox, J. B. Cross, V. Bakken, C. Adamo, J. Jaramillo, R. Gomperts, R. E. Stratmann, O. Yazyev, A. J. Austin, R. Cammi, C. Pomelli, J. W. Ochterski, R. L. Martin, K. Morokuma, V. G. Zakrzewski, G. A. Voth, P. Salvador, J. J. Dannenberg, S. Dapprich, A. D. Daniels, O. Farkas, J. B. Foresman, J. V. Ortiz, J. Cioslowski, and D. J. Fox, Gaussian, Inc., Wallingford CT, **2013**.
- 9 Y. Zhao, D. G. Truhlar, *Theor. Chem. Acc.* **2007**, *120*, 215.
- 10 T. Lu, F. Chen, *J. Comput. Chem.* **2012**, *33*, 580–592.
- 11 W. Humphrey, A. Dalke, K. Schulten, VMD: visual molecular dynamics. *J. Mol. Graph.* **1996**, *14*,
- 12 B. S. Brunschwig, J. Logan, M. D. Newton, N. Sutin, *J. Am. Chem. Soc.* **1980**, *102*, 5798.
- 13 J. L. Bredas, D. Beljonne, V. Coropceanu, J. Cornil, *Chem. Rev.* **2004**, *104*, 4971.
- 14 J. E. Norton, J. L. Bredas, *J. Am. Chem. Soc.* **2008**, *130*, 12377.
- 15 S. Di Motta, E. Di Donato, F. Negri, G. Orlandi, D. Fazzi, C. Castiglioni, *J. Am. Chem. Soc.* **2009**, *131*, 6591.

- 16 B. Zhang, Y.-H. Kan, Y. Geng, Y.-A. Duan, H.-B. Li, J. Hua, Z.-M. Su, *Org. Electron.* **2013**, *14*, 1359.
- 17 Y. Xu, C. Li, Z. Li, J. Wang, J. Xue, Q. Wang, X. Cai, Y. Wang, *CCS Chem.* **2022**, *4*, 2065–2079.
- 18 Q. Zhang, H. Kuwabara, W. J. Potscavage, S. Huang, Y. Hatae, T. Shibata, C. Adachi, *J. Am. Chem. Soc.* **2014**, *136*, 18070–18081.
- 19 Q. Zhang, B. Li, S. Huang, H. Nomura, H. Tanaka, C. Adachi, *Nat. Photonics* **2014**, *8*, 326–332.
- 20 T.-L. Wu, M.-J. Huang, C.-C. Lin, P.-Y. Huang, T.-Y. Chou, R.-W. Chen-Cheng, H.-W. Lin, R.-S. Liu, C.-H. Cheng, *Nat. Photonics* **2018**, *12*, 235–240.
- 21 T. Hatakeyama, K. Shiren, K. Nakajima, S. Nomura, S. Nakatsuka, K. Kinoshita, J. Ni, Y. Ono, T. Ikuta, *Adv. Mater.* **2016**, *28*, 2777–2781.
- 22 H. Kaji, H. Suzuki, T. Fukushima, K. Shizu, K. Suzuki, S. Kubo, T. Komino, H. Oiwa, F. Suzuki, A. Wakamiya, Y. Murata, C. Adachi, *Nat. Commun.* **2015**, *6*, 8476.
- 23 L. Fang, M. Li, W.-B. Lin, Y. Shen, C.-F. Chen, *Asian J. Org. Chem.* **2018**, *7*, 2518–2526.
- 24 Z. Domínguez, R. López-Rodríguez, E. Álvarez, S. Abbate, G. Longhi, U. Pischel, A. Ros, *Chem. Eur. J.* **2018**, *24*, 12660–12668.
- 25 Z.-H. Zhao, X. Liang, M.-X. He, M.-Y. Zhang, C.-H. Zhao, *Org. Lett.* **2019**, *21*, 9569–9573.
- 26 L. Fang, M. Li, W.-B. Lin, C.-F. Chen, *Tetrahedron* **2018**, *74*, 7164–7172.
- 27 L. Fang, M. Li, W.-B. Lin, Y. Shen, C.-F. Chen, *J. Org. Chem.* **2017**, *82*, 7402–7409.
- 28 H. Sakai, T. Kubota, J. Yuasa, Y. Araki, T. Sakanoue, T. Takenobu, T. Wada, T. Kawai, T. Hasobe, *J. Phys. Chem. C* **2016**, *120*, 7860–7869.
- 29 C. Shen, E. Anger, M. Srebro, N. Vanthuyne, L. Toupet, C. Roussel, J. Autschbach, R. Réau, J. Crassous, *Chem. Eur. J.* **2013**, *19*, 16722–16728.
- 30 K. Dhbaibi, L. Favereau, M. Srebro-Hooper, M. Jean, N. Vanthuyne, F. Zinna, B. Jamoussi, L. Di Bari, J. Autschbach, J. Crassous, *Chem. Sci.* **2018**, *9*, 735–742.
- 31 C. Shen, M. Srebro-Hooper, M. Jean, N. Vanthuyne, L. Toupet, J. A. G. Williams, A. R. Torres, A. J. Riives, G. Muller, J. Autschbach, J. Crassous, *Chem. Eur. J.* **2017**, *23*, 407–418.
- 32 N. Saleh, M. Srebro, T. Reynaldo, N. Vanthuyne, L. Toupet, V. Y. Chang, G. Muller, J. A. G. Williams, C. Roussel, J. Autschbach, J. Crassous, *Chem. Commun.* **2015**, *51*, 3754–3757.

- 33 N. Saleh, B. Moore, M. Srebro, N. Vanthuyne, L. Toupet, J. A. G. Williams, C. Roussel, K. K. Deol, G. Muller, J. Autschbach, J. Crassous, *Chem. Eur. J.* **2015**, *21*, 1673–1681.
- 34 C. Schaack, L. Arrico, E. Sidler, M. Górecki, L. Di Bari, F. Diederich, *Chem. Eur. J.* **2019**, *25*, 8003–8007.
- 35 C. Schaack, E. Sidler, N. Trapp, F. Diederich, *Chem. Eur. J.* **2017**, *23*, 14153–14157.
- 36 K. Dhbaibi, L. Favereau, M. Srebro-Hooper, C. Quinton, N. Vanthuyne, L. Arrico, T. Roisnel, B. Jamoussi, C. Poriel, C. Cabanetos, J. Autschbach, J. Crassous, *Chem. Sci.* **2020**, *11*, 567–576.
- 37 H. Sakai, S. Shinto, J. Kumar, Y. Araki, T. Sakanoue, T. Takenobu, T. Wada, T. Kawai, T. Hasobe, *J. Phys. Chem. C* **2015**, *119*, 13937–13947.
- 38 K. Yavari, W. Delaunay, N. De Rycke, T. Reynaldo, P. Aillard, M. Srebro-Hooper, V. Y. Chang, G. Muller, D. Tondelier, B. Geffroy, A. Voituriez, A. Marinetti, M. Hissler, J. Crassous, *Chem. Eur. J.* **2019**, *25*, 5303–5310.
- 39 R. Yamano, J. Hara, K. Murayama, H. Sugiyama, K. Teraoka, H. Uekusa, S. Kawauchi, Y. Shibata, K. Tanaka, *Org. Lett.* **2017**, *19*, 42–45.
- 40 R. Yamano, Y. Shibata, K. Tanaka, *Chem. Eur. J.* **2018**, *24*, 6364–6370.
- 41 H. Oyama, K. Nakano, T. Harada, R. Kuroda, M. Naito, K. Nobusawa, K. Nozaki, *Org. Lett.* **2013**, *15*, 2104.
- 42 C. Maeda, K. Nagahata, T. Shirakawa, T. Ema, *Angew. Chem. Int. Ed.* **2020**, *59*, 7813; *Angew. Chem.* **2020**, *132*, 7887–7891.
- 43 H. Oyama, M. Akiyama, K. Nakano, M. Naito, K. Nobusawa, K. Nozaki, *Org. Lett.* **2016**, *18*, 3654–3657.
- 44 T. Otani, A. Tsuyuki, T. Iwachi, S. Someya, K. Tateno, H. Kawai, T. Saito, K. S. Kanyiva, T. Shibata, *Angew. Chem. Int. Ed.* **2017**, *56*, 3906; *Angew. Chem.* **2017**, *129*, 3964–3968.
- 45 K. Goto, R. Yamaguchi, S. Hiroto, H. Ueno, T. Kawai, H. Shinokubo, *Angew. Chem. Int. Ed.* **2012**, *51*, 10333; *Angew. Chem.* **2012**, *124*, 10479–10482.
- 46 T. Matsuno, Y. Koyama, S. Hiroto, J. Kumar, T. Kawai, H. Shinokubo, *Chem. Commun.* **2015**, *51*, 4607–4610.
- 47 T. Otani, T. Sasayama, C. Iwashimizu, K. S. Kanyiva, H. Kawai, T. Shibata, *Chem. Commun.* **2020**, *56*, 4484–4487.

- 48 K. Murayama, Y. Oike, S. Furumi, M. Takeuchi, K. Noguchi, K. Tanaka, *Eur. J. Org. Chem.* **2015**, 1409–1414.
- 49 Y. Sawada, S. Furumi, A. Takai, M. Takeuchi, K. Noguchi, K. Tanaka, *J. Am. Chem. Soc.* **2012**, 134, 4080–4083.
- 50 S. Nishigaki, K. Murayama, Y. Shibata, K. Tanaka, *Mater. Chem. Front.* **2018**, 2, 585–590.
- 51 Y. Yamamoto, H. Sakai, J. Yuasa, Y. Araki, T. Wada, T. Sakanoue, T. Takenobu, T. Kawai, T. Hasobe, *J. Phys. Chem. C* **2016**, 120, 7421–7427.
- 52 Y. Yamamoto, H. Sakai, J. Yuasa, Y. Araki, T. Wada, T. Sakanoue, T. Takenobu, T. Kawai, T. Hasobe, *Chem. Eur. J.* **2016**, 22, 4263–4273.
- 53 L. Guy, M. Mosser, D. Pitrat, J.-C. Mлатier, M. Kukulka, M. Srebro-Hooper, E. Jeanneau, A. Bensalah-Ledoux, B. Baguenard, S. Guy, *J. Org. Chem.* **2019**, 84, 10870–10876.